# A new measurement of the Collins and Sivers asymmetries on a transversely polarised deuteron target

The COMPASS Collaboration

## Abstract

New high precision measurements of the Collins and Sivers asymmetries of charged hadrons produced in deep-inelastic scattering of muons on a transversely polarised $^6$LiD target are presented. The data were taken in 2003 and 2004 with the COMPASS spectrometer using the muon beam of the CERN SPS at 160 GeV/$c$. Both the Collins and Sivers asymmetries turn out to be compatible with zero, within the present statistical errors, which are more than a factor of 2 smaller than those of the published COMPASS results from the 2002 data. The final results from the 2002, 2003 and 2004 runs are compared with naive expectations and with existing model calculations.

# The COMPASS Collaboration

E.S. Ageev[24], V.Yu. Alexakhin[8], Yu. Alexandrov[18], G.D. Alexeev[8], M. Alexeev[29],
A. Amoroso[29], B. Badełek[30], F. Balestra[29], J. Ball[25], J. Barth[4], G. Baum[1], M. Becker[20],
Y. Bedfer[25], P. Berglund[13], C. Bernet[25], R. Bertini[29], M. Bettinelli[19] R. Birsa[28],
J. Bisplinghoff[3], P. Bordalo[15,a], F. Bradamante[28], A. Bressan[28], G. Brona[30], E. Burtin[25],
M.P. Bussa[29], V.N. Bytchkov[8], A. Chapiro[27], A. Cicuttin[27], M. Colantoni[29,b],
A.A. Colavita[27], S. Costa[29,c], M.L. Crespo[27], N. d'Hose[25], S. Dalla Torre[28], S. Das[7],
S.S. Dasgupta[6], R. De Masi[20], N. Dedek[19], D. Demchenko[16], O.Yu. Denisov[29,d],
L. Dhara[7], V. Diaz[28,27], A.M. Dinkelbach[20], S.V. Donskov[24], V.A. Dorofeev[24],
N. Doshita[2,21], V. Duic[28], W. Dünnweber[19], A. Efremov[8], P.D. Eversheim[3], W. Eyrich[9],
M. Faessler[19], V. Falaleev[11], P. Fauland[1], A. Ferrero[29], L. Ferrero[29], M. Finger[22],
M. Finger jr.[8], H. Fischer[10], J. Franz[10], J.M. Friedrich[20], V. Frolov[29,d], U. Fuchs[11],
R. Garfagnini[29], F. Gautheron[1], O.P. Gavrichtchouk[8], S. Gerassimov[18,20], R. Geyer[19],
M. Giorgi[28], B. Gobbo[28], S. Goertz[2,4], A.M. Gorin[24], O.A. Grajek[30], A. Grasso[29],
B. Grube[20], A. Guskov[8], F. Haas[20], J. Hannappel[4,16], D. von Harrach[16], T. Hasegawa[17],
S. Hedicke[10], F.H. Heinsius[10], R. Hermann[16], C. Heß[2], F. Hinterberger[3],
M. von Hodenberg[10], N. Horikawa[21,e], S. Horikawa[21], I. Horn[3], C. Ilgner[11,19],
A.I. Ioukaev[8], S. Ishimoto[21], I. Ivanchin[8], O. Ivanov[8], T. Iwata[21,f], R. Jahn[3], A. Janata[8],
R. Joosten[3], N.I. Jouravlev[8], E. Kabuß[16], V. Kalinnikov[28], D. Kang[10], B. Ketzer[20],
G.V. Khaustov[24], Yu.A. Khokhlov[24], Yu. Kisselev[1,2], F. Klein[4], K. Klimaszewski[30],
S. Koblitz[16], J.H. Koivuniemi[2,13], V.N. Kolosov[24], E.V. Komissarov[8], K. Kondo[2,21],
K. Königsmann[10], I. Konorov[18,20], V.F. Konstantinov[24], A.S. Korentchenko[8],
A. Korzenev[16,d], A.M. Kotzinian[8,29], N.A. Koutchinski[8], O. Kouznetsov[8], K. Kowalik[30],
D. Kramer[14], N.P. Kravchuk[8], G.V. Krivokhizhin[8], Z.V. Kroumchtein[8], J. Kubart[14],
R. Kuhn[20], V. Kukhtin[8], F. Kunne[25], K. Kurek[30], M.E. Ladygin[24], M. Lamanna[11,28],
J.M. Le Goff[25], M. Leberig[11,16], A.A. Lednev[24], A. Lehmann[9], J. Lichtenstadt[26],
T. Liska[23], I. Ludwig[10], A. Maggiora[29], M. Maggiora[29], A. Magnon[25], G.K. Mallot[11],
C. Marchand[25], J. Marroncle[25], A. Martin[28], J. Marzec[31], L. Masek[14], F. Massmann[3],
T. Matsuda[17], D. Matthiä[10], A.N. Maximov[8], W. Meyer[2], A. Mielech[28,30],
Yu.V. Mikhailov[24], M.A. Moinester[26], T. Nagel[20], O. Nähle[3], J. Nassalski[30], S. Neliba[23],
D.P. Neyret[25], V.I. Nikolaenko[24], A.A. Nozdrin[8], V.F. Obraztsov[24], A.G. Olshevsky[8],
M. Ostrick[4,16], A. Padee[31], P. Pagano[28], S. Panebianco[25], D. Panzieri[29,b], S. Paul[20],
D.V. Peshekhonov[8], V.D. Peshekhonov[8], G. Piragino[29], S. Platchkov[11,25],
K. Platzer[19], J. Pochodzalla[16], J. Polak[14], V.A. Polyakov[24], G. Pontecorvo[8], A.A. Popov[8],
J. Pretz[4], S. Procureur[25], C. Quintans[15], S. Ramos[15,a], G. Reicherz[2], A. Richter[9],
E. Rondio[30], A.M. Rozhdestvensky[8], D. Ryabchikov[24], V.D. Samoylenko[24], A. Sandacz[30],
H. Santos[15], M.G. Sapozhnikov[8], I.A. Savin[8], P. Schiavon[28], C. Schill[10], L. Schmitt[20],
P. Schönmeier[9], W. Schroeder[9], D. Seeharsch[20], M. Seimetz[25], D. Setter[10],
O.Yu. Shevchenko[8], H.-W. Siebert[12,4], L. Silva[15], L. Sinha[7], A.N. Sissakian[8],
M. Slunecka[8], G.I. Smirnov[8], F. Sozzi[28], A. Srnka[5], F. Stinzing[9], M. Stolarski[30],
V.P. Sugonyaev[24], M. Sulc[14], R. Sulej[31], V.V. Tchalishev[8], S. Tessaro[28], F. Tessarotto[28],
A. Teufel[9], L.G. Tkatchev[8], T. Toeda[21], S. Trippel[10], G. Venugopal[3], M. Virius[23],
N.V. Vlassov[8], M. Wagner[9], R. Webb[9], E. Weise[3,10], Q. Weitzel[20], R. Windmolders[4],
W. Wiślicki[30], A.M. Zanetti[28], K. Zaremba[31], M. Zavertyaev[18], J. Zhao[16,25], R. Ziegler[3],
and A. Zvyagin[19]

1) Universität Bielefeld, Fakultät für Physik, 33501 Bielefeld, Germany[g]

2) Universität Bochum, Institut für Experimentalphysik, 44780 Bochum, Germany[g]

3) Universität Bonn, Helmholtz-Institut für Strahlen- und Kernphysik, 53115 Bonn, Germany[g]

4) Universität Bonn, Physikalisches Institut, 53115 Bonn, Germany[g]

5) Institute of Scientific Instruments, AS CR, 61264 Brno, Czech Republic[h]

6) Burdwan University, Burdwan 713104, India[j]

7) Matrivani Institute of Experimental Research & Education, Calcutta-700 030, India[k]

8) Joint Institute for Nuclear Research, 141980 Dubna, Moscow region, Russia

9) Universität Erlangen–Nürnberg, Physikalisches Institut, 91054 Erlangen, Germany[g]

10) Universität Freiburg, Physikalisches Institut, 79104 Freiburg, Germany[g]

11) CERN, 1211 Geneva 23, Switzerland

12) Universität Heidelberg, Physikalisches Institut, 69120 Heidelberg, Germany[g]

13) Helsinki University of Technology, Low Temperature Laboratory, 02015 HUT, Finland and University of Helsinki, Helsinki Institute of Physics, 00014 Helsinki, Finland

14) Technical University in Liberec, 46117 Liberec, Czech Republic[h]

15) LIP, 1000-149 Lisbon, Portugal[i]

16) Universität Mainz, Institut für Kernphysik, 55099 Mainz, Germany[g]

17) University of Miyazaki, Miyazaki 889-2192, Japan[l]

18) Lebedev Physical Institute, 119991 Moscow, Russia

19) Ludwig-Maximilians-Universität München, Department für Physik, 80799 Munich, Germany[g]

20) Technische Universität München, Physik Department, 85748 Garching, Germany[g]

21) Nagoya University, 464 Nagoya, Japan[l]

22) Charles University, Faculty of Mathematics and Physics, 18000 Prague, Czech Republic[h]

23) Czech Technical University in Prague, 16636 Prague, Czech Republic[h]

24) State Research Center of the Russian Federation, Institute for High Energy Physics, 142281 Protvino, Russia

25) CEA DAPNIA/SPhN Saclay, 91191 Gif-sur-Yvette, France

26) Tel Aviv University, School of Physics and Astronomy, 69978 Tel Aviv, Israel[m]

27) INFN Trieste and ICTP–INFN MLab Laboratory, 34014 Trieste, Italy

28) INFN Trieste and University of Trieste, Department of Physics, 34127 Trieste, Italy

29) INFN Turin and University of Turin, Physics Department, 10125 Turin, Italy

30) Sołtan Institute for Nuclear Studies and Warsaw University, 00-681 Warsaw, Poland[n]

31) Warsaw University of Technology, Institute of Radioelectronics, 00-665 Warsaw, Poland[o]

a) Also at IST, Universidade Técnica de Lisboa, Lisbon, Portugal

b) Also at University of East Piedmont, 15100 Alessandria, Italy

c) deceased

d) On leave of absence from JINR Dubna

e) Also at Chubu University, Kasugai, Aichi, 487-8501 Japan

f) Also at Yamagata University, Yamagata, 992-8510 Japan

g) Supported by the German Bundesministerium für Bildung und Forschung

h) Suppported by Czech Republic MEYS grants ME492 and LA242

i) Supported by the Portuguese FCT - Fundação para a Ciência e Tecnologia grants POCTI/FNU/49501/2002 and POCTI/FNU/50192/2003

j) Supported by DST-FIST II grants, Govt. of India

k) Supported by the Shailabala Biswas Education Trust

l) Supported by the Ministry of Education, Culture, Sports, Science and Technology, Japan; Daikou Foundation and Yamada Foundation

1

**Contents**

# 1    An introduction to transverse spin physics

## 1.1    Historical introduction

The importance of transverse spin effects at high energy in hadronic physics was first suggested by the discovery in 1976 that $\Lambda$ hyperons produced in $pN$ interactions exhibited an anomalously large transverse polarisation [1]. This effect could not be easily explained. For a long time it was believed to be forbidden at leading twist in QCD [2], and very little theoretical work was devoted to this field for more than a decade. Nevertheless some important theoretical progress for the understanding of single spin asymmetry (SSA) phenomena was done at that time [3].

This situation changed in the nineties. After the first hints of large single transverse spin asymmetries in inclusive $\pi^0$ production in polarised pp scattering at CERN [4] and in IHEP [5], remarkably large asymmetries were found at Fermilab both for neutral and charged pions [6]. The discovery of the EMC collaboration at CERN in the late eighties that the quark spin contributes only a small fraction to the proton spin [7] caused a renewed interest in the origin of the nucleon spin and proposals for new and versatile experiments. In parallel, intense theoretical activity was taking place: the significance of the quark transversity distribution, already introduced in 1979 [8] to describe a quark in a transversely polarised nucleon, was reappraised [9] in 1990, and its measurability via the Drell–Yan process established. In 1991 a general scheme of all leading twist and higher-twist parton distribution functions was worked out [10], and in 1993 a way to measure transversity in lepton nucleon polarised deep-inelastic scattering (DIS) was suggested [11]. On the experimental side, the RHIC-Spin Collaboration [12] and the HELP Collaboration [13] put forward the first proposals to measure transversity. Today transversity is an important part of the scientific programme of the HERMES experiment at DESY, of the RHIC experiments at BNL, and of the COMPASS experiment at CERN, all presently taking data. An experiment to measure transversity is being prepared at JLAB. First results on a transversely polarised proton target have been published recently by the HERMES Collaboration [14] and, on a transversely polarised deuteron target by COMPASS [15].

The COMPASS published results refer to the data taken in 2002. Further data taking occurred in 2003 and 2004, and in this paper results from these new data are presented, as well as a reanalysis of the 2002 data and the final results for the 2002–2004 data.

## 1.2    The Collins mechanism

To fully specify the quark structure of the nucleon at the twist-two level, the transverse spin distributions $\Delta_T q(x)$ must be added to the momentum distributions $q(x)$ and the helicity distributions $\Delta q(x)$ [10], where $x$ is the Bjorken variable. For a discussion on notation, see Ref. [16]. If the quarks are collinear with the parent nucleon (no intrinsic quark transverse momentum $\vec{k}_T$), or after integration over $\vec{k}_T$, these three distributions exhaust the information on the internal dynamics of the nucleon. More distributions are allowed admitting a finite $\vec{k}_T$, as we will see in Sections 1.3 and 1.4, or at higher twist [16–19].

The distributions $\Delta_T q$ are difficult to measure, since they are chirally odd and therefore absent in inclusive DIS. They may instead be extracted from measurements of the single-spin asymmetries in cross-sections for semi-inclusive DIS (SIDIS) of leptons on transversely polarised nucleons, in which a hadron is also detected in the final state. In these processes the measurable asymmetry is due to the combined effect of $\Delta_T q$ and another chirally-odd function which describes the spin-dependent part of the hadronisation of a transversely polarised quark $q$ into a hadron $h$.

The existence of an azimuthal asymmetry in transversely polarised leptoproduction of spinless hadrons at leading twist, which depends on a $T$-odd fragmentation function and arises
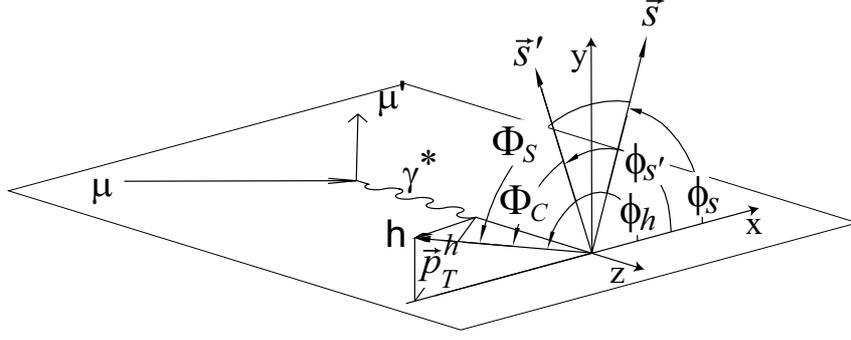
3

Figure 1: Definition of the Collins and Sivers angles. The vectors $\vec{p}_T^h$, $\vec{s}$ and $\vec{s'}$ are the hadron transverse momentum and spin of the initial and struck quarks respectively.

from final-state interaction effects, was predicted by Collins [11] and is now generally known as the Collins effect. It is responsible for a left-right asymmetry in the fragmentation of transversely polarised quarks. In some models [20], the Collins asymmetry is expected to be largest for the leading hadron in the current jet, i.e. the hadron with the highest momentum.

Assuming the detected hadron to be spinless, and a collinear quark distribution in the nucleon, at leading twist the SIDIS cross-section can be written as

$$
\frac{d\sigma}{dx\,dy\,dz\,d^2p_T^h\,d\phi_S} = \frac{2\alpha_{\text{em}}^2 s}{Q^4} \sum_q e_q^2 \cdot \left\{ \frac{1}{2}\left[1 + (1-y)^2\right] \cdot x \cdot q(x) \cdot D_q^h(z, p_T^h) + \right.
$$

$$
\left. + (1-y)\,|\vec{S}_\perp|\,\sin(\phi_h - \phi_{s'}) \cdot x \cdot \Delta_T q(x) \cdot \Delta_T^0 D_q^h(z, p_T^h) \right\}
\tag{1}
$$

where Bjorken $x$ is $Q^2/[2M(E_l - E_{l'})]$, $y$ is the fractional energy of the virtual photon, $Q^2$ the photon virtuality, $M$ the target nucleon mass, and $z = E_h/(E_l - E_{l'})$ the fraction of available energy carried by the hadron. The energies $E_h$, $E_l$, and $E_{l'}$ are the energies of the hadron, the incoming lepton, and the scattered lepton respectively in the target rest frame system. The hadron transverse momentum $\vec{p}_T^h$ is evaluated with respect to the virtual photon direction. Referring to Fig. 1, $\phi_h$ and $\phi_{s'}$ are the azimuthal angles of the hadron and of the struck quark spin in a coordinate system in which the z-axis is the virtual photon direction, and the x-z plane is the lepton scattering plane with positive x-direction along the scattered lepton transverse momentum. $\vec{S}_\perp$ is the target spin normal to the virtual photon direction and $\phi_S$ is its azimuthal angle with respect to the lepton scattering plane.

The $\vec{p}_T^h$-dependent fragmentation function can be obtained by investigating the fragmentation of a polarised quark $q$ into a hadron $h$, and is expected to be of the form

$$
D_{Tq}^h(z, \vec{p}_T^h) = D_q^h(z, p_T^h) + \Delta_T^0 D_q^h(z, p_T^h) \cdot \sin(\phi_h - \phi_{s'}).
\tag{2}
$$

where $\Delta_T^0 D_q^h(z, p_T^h)$ is the $T$-odd part of the fragmentation function, responsible for the left-right asymmetry in the fragmentation of the transversely polarised quark.

The "Collins angle" $\Phi_C$ was originally defined in [11] as the angle between the transverse momentum of the outgoing hadron and the transverse spin vector of the fragmenting quark, i.e.,

$$
\sin \Phi_C = \frac{(\vec{p}_T^h \times \vec{q}) \cdot \vec{s'}}{|\vec{p}_T^h \times \vec{q}|\,|\vec{s'}|} .
\tag{3}
$$

or

$$
\Phi_C = \phi_h - \phi_{s'} .
\tag{4}
$$

4

Since, as dictated by QED, the directions of the final and initial quark spins are related to each other by $\phi_{s'} = \pi - \phi_s$ , equation (4) becomes

$$\Phi_C = \phi_h + \phi_S - \pi \,.$$ (5)

By comparing the cross-sections on oppositely polarised target nucleons one obtains from expression (1) the transverse single spin asymmetry

$$A_T^h \equiv \frac{d\sigma(\vec{S}_\perp) - d\sigma(-\vec{S}_\perp)}{d\sigma(\vec{S}_\perp) + d\sigma(-\vec{S}_\perp)} = |\vec{S}_\perp| \cdot D_{NN} \cdot A_{Coll} \cdot \sin \Phi_C$$ (6)

where the "Collins asymmetry" is

$$A_{Coll} = \frac{\sum_q e_q^2 \cdot \Delta_T q(x) \cdot \Delta_T^0 D_q^h(z, p_T^h)}{\sum_q e_q^2 \cdot q(x) \cdot D_q^h(z, p_T^h)} \,,$$ (7)

and

$$D_{NN} = \frac{1-y}{1-y+y^2/2}$$ (8)

is the transverse spin transfer coefficient from the initial to the struck quark [16].

## 1.3 The Sivers mechanism

An entirely different mechanism was suggested by Sivers [21] as a possible cause of the transverse spin effects observed in pp scattering. This mechanism could also be responsible for a spin asymmetry in the cross-section of SIDIS of leptons on transversely polarised nucleons. Sivers conjecture was the possible existence of a correlation between the transverse momentum $\vec{k}_T$ of an unpolarised quark in a transversely polarised nucleon and the nucleon polarisation vector, i.e. that the quark distribution $q(x)$ in expression (1) could be written as

$$q_T(x, \vec{k}_T) = q(x, k_T) + |\vec{S}_\perp| \cdot \Delta_0^T q(x, k_T) \cdot \sin \Phi_S$$ (9)

where the "Sivers angle"

$$\Phi_S = \phi_q - \phi_S$$ (10)

is the relative azimuthal angle between the quark transverse momentum $\vec{k}_T$ and the target spin $\vec{S}_\perp$.

Under the assumption that the hadron produced in the fragmentation and the fragmenting quark are collinear, i.e. that all the hadron transverse momentum originates from the intrinsic transverse momentum of the quark in the nucleon ($\vec{p}_T^h = z\vec{k}_T$), the Sivers angle, shown in Fig. 1, becomes

$$\Phi_S = \phi_h - \phi_S$$ (11)

and the SIDIS cross-section in leading order QCD is given by

$$\frac{d\sigma}{dx\,dy\,dz\,d^2p_T^h\,d\phi_S} = \frac{2\alpha_{em}^2 s}{Q^4} \sum_q e_q^2 \cdot \frac{1}{2} \left[ 1 + (1-y)^2 \right] \cdot x \cdot$$

$$\cdot \left[ q(x, p_T^h/z) + |\vec{S}_\perp| \sin(\Phi_S) \Delta_0^T q(x, p_T^h/z) \right] \cdot D_q^h(z) \,.$$ (12)

5

Comparing the cross-sections on oppositely polarised target nucleons, the transverse spin asymmetry of expression (6) becomes

$$A_T^h \equiv \frac{d\sigma(\vec{S}_\perp) - d\sigma(-\vec{S}_\perp)}{d\sigma(\vec{S}_\perp) + d\sigma(-\vec{S}_\perp)} = |\vec{S}_\perp| \cdot A_{Siv} \cdot \sin \Phi_S \tag{13}$$

where the "Sivers asymmetry"

$$A_{Siv} = \frac{\sum_q e_q^2 \cdot \Delta_0^T q(x, p_T^h/z) \cdot D_q^h(z)}{\sum_q e_q^2 \cdot q(x, p_T^h/z) \cdot D_q^h(z)} \tag{14}$$

could be revealed as a $\sin \Phi_S$ modulation in the number of produced hadrons.

The existence of the Sivers function requires final/initial state interaction, and an interference between different helicity Fock states. In the absence of interactions the Sivers function would vanish by time-reversal invariance of QCD (see e.g. Ref. [19]) and indeed it was believed for several years that the Sivers function is zero. Recently it was shown however [22–24] that these interactions are represented naturally by the gauge link that is required for a gauge invariant definition of a transverse momentum dependent (TMD) parton distribution, thus the Sivers function has become a very important piece in the most fundamental issues of QCD.

## 1.4  More general formalism

A combined treatment of the the Collins and Sivers mechanisms requires a more general approach and the introduction of TMD distributions and fragmentation functions [18, 19, 25]. Convolution integrals appear in the SIDIS cross-section, whose expression becomes

$$d\sigma \sim \sum_q e_q^2 \cdot \left\{ \frac{1}{2} \left[ 1 + (1-y)^2 \right] x \left[ q \otimes D_q^h + |\vec{S}_\perp| \sin(\Phi_S) \Delta_0^T q \otimes D_q^h \right] + \right.$$
$$\left. + (1-y) |\vec{S}_\perp| \sin(\Phi_C) x \Delta_T q \otimes \Delta_T^0 D_q^h \right\} . \tag{15}$$

In the general expression of the SIDIS cross-section at leading order QCD other terms related to different single and double spin azimuthal asymmetries appear. Here they are neglected since they are beyond the scope of this paper. The symbol $\otimes$, which replaces the products in Eq. (1) and (12), indicates the convolution integral

$$DF \otimes FF = \int d^2 k_T \; DF(x, \vec{k}_T) \cdot FF(z, \vec{p}_T^h - z\vec{k}_T) \tag{16}$$

where $DF$ and $FF$ are generic TMD distributions and fragmentation functions respectively.

The transverse spin asymmetry is then given by

$$\begin{aligned} A_T^h &\equiv \frac{d\sigma(\vec{S}_\perp) - d\sigma(-\vec{S}_\perp)}{d\sigma(\vec{S}_\perp) + d\sigma(-\vec{S}_\perp)} \\ &= |\vec{S}_\perp| \cdot D_{NN} \, A_{Coll} \cdot \sin \Phi_C + |\vec{S}_\perp| \cdot A_{Siv} \cdot \sin \Phi_S \end{aligned} \tag{17}$$

where the Collins and the Sivers asymmetries are still given by Eq. (7) and (14) when replacing the products of the distribution and fragmentation functions with the corresponding convolutions. In the usual assumption of Gaussian distributions for the parton and the hadron transverse momenta in the $DF$ and in the $FF$, the only effect of the convolution integral in Eq. (7) and (14) is the presence of a factor which depends on $< \vec{k}_T^2 >$ and $< \vec{p}_T^{h\,2} >$ (see f.i. [26, 27]).

Since the Collins and Sivers terms in the transverse spin asymmetry depend on the two independent angles $\Phi_C$ and $\Phi_S$, measuring SIDIS on a transversely polarised target allows the Collins and the Sivers effects to be disentangled and the two asymmetries can separately be extracted from the data.

## 2 The COMPASS experiment

### 2.1 Physics objectives

The COMPASS experiment was proposed to CERN in 1996 to investigate hadron structure and hadron spectroscopy by carrying on a number of key measurements using both hadron ($\pi$, K and protons) and muon high-energy beams. Apart from a short pilot run in 2004 with 190 GeV/$c$ pions to measure the pion polarisability via Primakoff scattering on high-Z targets, the experiment in so far has focused on the investigation of the spin structure of the nucleon using a 160 GeV/$c$ $\mu^+$ beam and a polarised deuteron target. In the longitudinal target spin mode, the main goal of the experiment is the measurement of $\Delta G/G$ [28], the polarisation of the gluons in a longitudinally polarised nucleon, but very precise $A_1^d$ data are also collected [29]. In about 20% of the running time, the target polarisation was set along the vertical direction, orthogonal to the beam axis, and transverse spin effects were measured, which are the subject of this paper.

### 2.2 The experimental set-up

The COMPASS spectrometer [30] has been set up in the CERN SPS North Area.

The layout of the spectrometer which was on the floor in 2003 is shown in Fig. 2. To combine large geometrical acceptance and broad dynamical range, the spectrometer comprises two magnetic stages, and is made up of a variety of tracking detectors, a fast RICH, two hadronic calorimeters, and provides muon identification via filtering through thick absorbers.

The first stage is centred around the spectrometer magnet SM1 (1 Tm bending power) and the design acceptance is about $\pm 200$ mrad in both planes, to fully contain the hadrons of the current jet. The second stage uses the spectrometer magnet SM2 (operated at a bending power of 4.4 Tm), located 18 m downstream from the target, and the acceptance is $\pm 50$ and $\pm 25$ mrad in the horizontal and vertical plane respectively.

The design of detector components, electronics and data acquisition system allows to handle beam rates up to $10^8$ muons/s and about $5 \cdot 10^7$ hadrons/s. The triggering system and the tracking system of COMPASS have been designed to stand the associated rate of secondaries, and use state-of-the-art detectors. Also, fast front-end electronics, multi-buffering, and a large
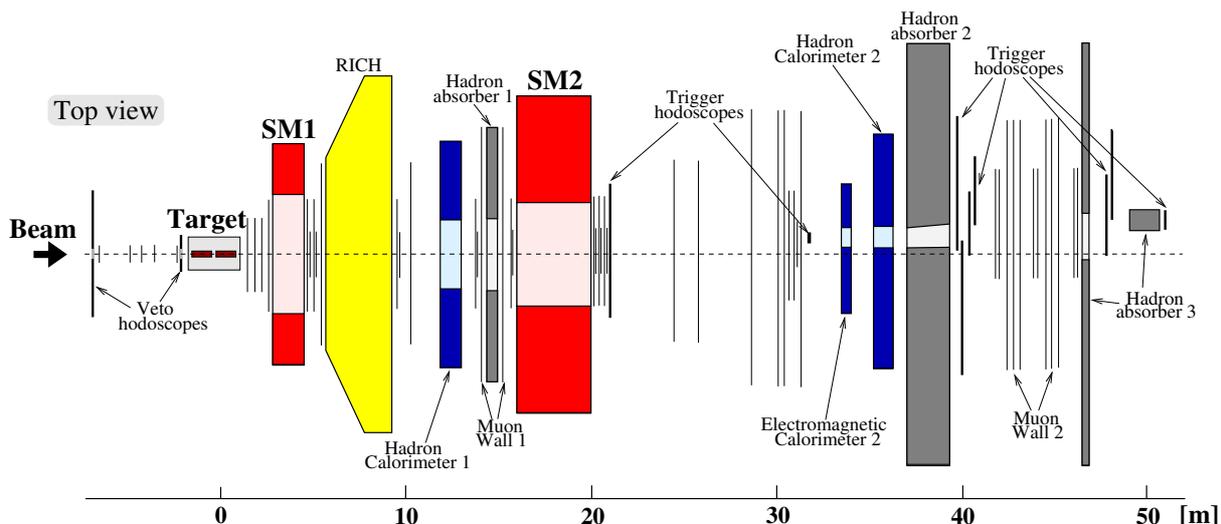


Figure 2: Top view of the lay-out of the spectrometer for the COMPASS experiment in 2003. The labels and the arrows refer to the major components of the trigger and PID systems. The thin vertical lines represent the tracking detectors.

and fast storage of events are essential.

The experiment has been run at a muon energy of 160 GeV. The muons originate from the decay of $\pi$ and K mesons produced by the 400 GeV proton beam on a primary beryllium target. The $\mu^+$ beam is naturally polarised by the weak decay mechanism, and the beam polarisation is about -80%. The beam polarisation contributes to the transverse spin dependent part of the cross-section only by higher twist effects, which are not considered in the leading-order analysis of this paper. The $\mu^+$ intensity is $2 \cdot 10^8$ per spill of 4.8 s with a cycle time of 16.8 s. The beam profile presents a Gaussian core and a large non-Gaussian tail due to halo muons. The beam has a nominal energy of 160 GeV and is focused at the target centre, with a spread of 7 mm (r.m.s.) and a momentum spread of $\sigma_p/p = 0.05$ for the Gaussian core. The momentum of each muon is measured upstream of the experimental area in a beam momentum station consisting of several planes of scintillator strips with 3 dipole magnets (30 Tm total bending power) in between. The precision of the momentum determination is typically $\Delta p/p \leq 0.003$.

Due to the major problems and delay in the construction of the new large-acceptance COMPASS polarised target (PT) magnet, the experiment has utilised in so far the magnet from the SMC experiment, which has a similar design and identical magnetic properties, but a smaller bore (26.5 cm diameter). The resulting angular acceptance is reduced, going from $\pm 170$ mrad at the downstream end to $\pm 69$ mrad at the upstream end of the target. The polarised target system [31] consists of two oppositely polarised target cells (upstream $u$, downstream $d$), 60 cm long each and 3 cm diameter, so that data are collected simultaneously for the two target spin orientations. The PT magnet can provide both a solenoidal field (2.5 T) and a dipole field for adiabatic spin rotation (up to 0.5 T) and for the transversity measurements (set at 0.42 T). Correspondingly, the target polarisation can then be oriented either longitudinally or transversely to the beam direction. The target is cooled to temperatures below 100 mK by a $^3$He-$^4$He dilution refrigerator. When operated in the frozen spin mode, temperatures of $\sim$50 mK are reached. The polarisation was lost at rate of 0.4 - 1.0%/day in the 0.42 T dipole field and 0.05 - 0.1%/day in 2.5 T solenoid field. The use of two different target materials, $NH_3$ as proton target and $^6$LiD as deuteron target, is foreseen. Polarisations of 90% [32] and 50% [30] have been reached, respectively. In so far only $^6$LiD has been used as target: its favourable dilution factor of $\sim$0.4 is of the utmost importance for the measurement of $\Delta G$. The dynamical nuclear polarisation system can polarise the target only at 2.5 T, i.e. in the solenoidal field. To run in the transverse polarisation mode, the spins are frozen and rotated adiabatically by first lowering the longitudinal field to 0.5 T, then rotating the magnetic field to the vertical direction with the help of the dipole coils. The polarisation values are obtained from corresponding measurements done at the beginning and at the end of each data taking period, with the polarised target field set back at 2.5 T, and take into account the relaxation time of the target polarisation.

To match the expected particle flux in the various locations along the spectrometer, COMPASS uses very different tracking detectors. The small area trackers consist of several stations of scintillating fibres, silicon detectors, micromegas chambers [33] and gaseous chambers using the GEM-technique [34]. Large area tracking devices are made from gaseous detectors (Drift Chambers, Straw tubes [35], and MWPC's) placed around the two spectrometer magnets.

Muons are identified in large-area Iarocci-like tubes and drift tubes downstream of muon absorbers. Hadrons are detected by two large iron-scintillator sampling calorimeters, installed in front of the absorbers and shielded to avoid electromagnetic contamination. The charged particles identification relies on the RICH technology [36]. In this paper we have not utilised the information of the RICH, and give results for non-identified hadron asymmetries only. The asymmetries for RICH-identified hadrons (pions and kaons) will be the subject of a separate paper.
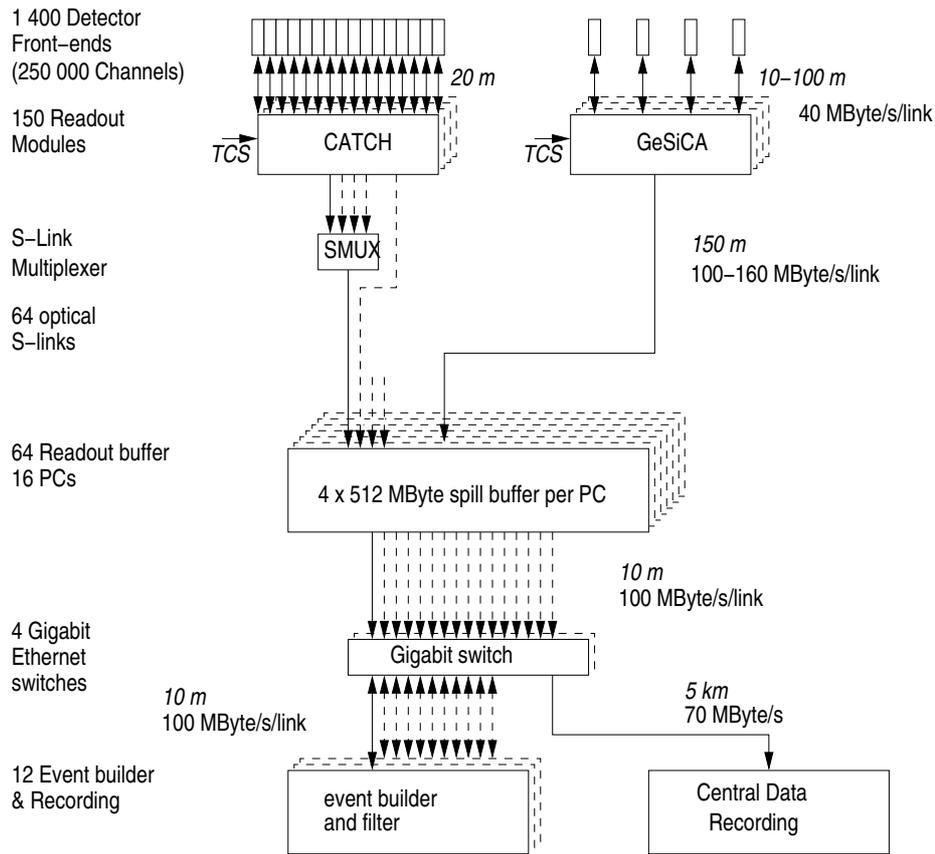
Figure 3: General architecture of the DAQ system.

The trigger [37] is formed by a combination of signals indicating the presence of a scattered muon at a given angle or in a given energy range. In most DIS events ($Q^2 > 1$ (GeV/$c$)$^2$), the scattered muon is identified by coincidence signals in the trigger hodoscopes, that measure the projection of the scattering angle in the non-bending plane and check its compatibility with the target position Several veto counters installed upstream of the target are used to avoid triggers due to halo muons. In addition to this inclusive trigger mode, several semi-inclusive triggers select events fulfilling requirements based on the muon energy loss and on the presence of a hadron signal in the calorimeters. The acceptance is further extended toward high $Q^2$ values by the addition of a standalone calorimetric trigger in which no condition is set for the scattered muon.

A complete description of the spectrometer can be found in Ref. [30].

## 2.3 Data taking and off-line system

The data acquisition system [38] was designed to read the 250 000 detector channels with an event rate of up to 100 kHz and with essentially no dead-time. This required a full custom design of the readout electronics (mounted directly on the detectors) and of the readout-driver modules (named CATCH and GeSiCA), which perform local event building and trigger distribution to the front-end boards (Fig. 3). The trigger control system (TCS) performs trigger distribution and synchronisation of the time-to-digital converters to better than 50 ps. The data collected during the 4.8 s spills is stored in 32 GByte buffers. The event building is performed on high performance Linux PCs connected to the read out system via Gigabit Ethernet. The data are grouped in "runs" corresponding to about 100 consecutive spills in 2003 and 200 in
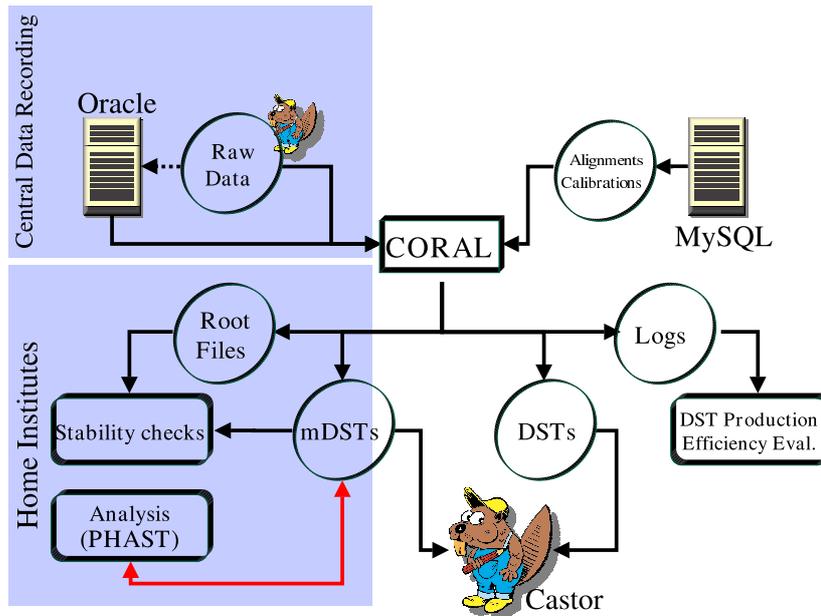
Figure 4: Schematic view of the off-line system and reconstruction and analysis flow.

2004. General information on the run is extracted and stored in the meta-data tables of an Oracle database. The files are then sent to the Central Data Recording facility in the CERN computer centre in parallel multiple streams over a dedicated optical fibre network at an average speed of 70 MBytes/s.

Once at the computer centre, the files are registered in the name space of CASTOR (the CERN hierarchical storage management system): from this moment onward, CASTOR controls thoroughly the events data handling (copy to tape, managing of the disk space), while an Oracle RAC database system is in charge of translating high-level requests of data into file requests. The huge amount of data of about 350 TBytes/year is reconstructed at the CERN computer centre, requiring a computing power of about 200k SPECint2000. The event reconstruction is carried on by CORAL, the COMPASS reconstruction and analysis framework, a fully object-oriented program with a modular architecture written in C++, which provides interfaces for the event reconstruction algorithms and insulation layers to access the data and for external pluggable packages [39]. The reconstruction is carried out in parallel, by some 600 jobs running on the CERN batch system. CORAL decodes the data, reconstructs tracks and vertexes, and performs the particle identification making use of the alignment and calibration data describing the apparatus, which are stored as time/version-dependent information in a MySql database. The reconstructed data is output in a proprietary format to files called Data Summary Tapes (DSTs), and in ROOT [40] format to mini-DSTs, which are selectively filtered out from the DSTs during production and turn out to have a size of about 1% of the original RAW data. DSTs and miniDSTs are stored also centrally on tape, under CASTOR. The physics analysis is performed on the mini-DSTs, replicated in the different institutes, by means of PHAST, the COMPASS framework for the final data analysis [39]. Fig. 4 depicts the reconstruction and analysis system to which the data flow after they are stored centrally. For the simulations, the Monte Carlo program COMGeant [39], based on GEANT 3 and LEPTO 6.5.1, has been written and used extensively.

10

In the first three years of data taking, from 2002 to 2004, in which the experiment benefited of about $12 \cdot 10^5$ spills, COMPASS collected 30 billion events, corresponding to a total data sample of more than 1 PByte. Thanks to continuous work on alignment and improvement of the reconstruction code, these data have been processed several times. About 20% of these data have been taken in the transverse target spin mode.

## 2.4 Principle of the measurement

As explained in Section 1.1, the Collins and the Sivers asymmetries can be estimated from the SIDIS data by measuring, in a given kinematical bin defined by $x$, $z$, or $p_T^h$, the number of events $N^+$ and $N^-$ collected on oppositely polarised target nucleons, and fitting the measured asymmetries $(N^+ - N^-)/(N^+ - N^-)$ either with a $\sin \Phi_C$ or a $\sin \Phi_S$ dependence. Since the spectrometer acceptance is somewhat different for the two target halves, the cross-section asymmetries cannot be obtained from a direct comparison of the number of events collected in the $u-$ and $d-$cell. It is necessary to compare the number of events collected in each cell with the two target spin orientations, and the two-cell system allows to reduce the systematic effects.

The orientation of the target polarisation cannot be flipped fast in the COMPASS target system. The holding field is 0.42 T, and transverse to the beam, thus it is out of question to flip the target spin by inverting the magnetic field because the acceptance would change. Polarisation reversal is done by exchanging the microwave frequencies for $u-$ and $d-$cells, and to achieve $\sim$50% polarisation one needs two days. Therefore, once the target is polarised, data are taken for several days (typically 5) before a polarisation reversal is done, and to evaluate an asymmetry one compares the number of events collected almost a week apart. For this reason, the transverse spin measurement usually was carried out at the end of the run, when the spectrometer was fully operational and functioning smoothly, and great care was taken not to intervene on any detector to avoid changes in efficiency.

The typical cycle (a data taking period) consisted therefore of 5 days of measurement in one configuration (yielding f.i. $N_u^+$ and $N_d^-$), 2 days to change the target polarisation, and 5 more days of data taking in the opposite configuration (yielding $N_u^-$ and $N_d^+$). At this point, one can estimate the cross-section asymmetry. A straightforward procedure was used for the published 2002 data analysis [15], namely to derive one asymmetry from $N_u^+$ and $N_u^-$, a second asymmetry from $N_d^+$ and $N_d^-$, check their consistency and then average the two. A different method, which uses at once the four numbers and is less sensitive to differences in acceptance, has been used in this analysis, and is described in Section 4.3.2.

In this paper final results are presented for all the data collected with the deuteron target in the three years 2002–2003–2004. Data were collected during two periods in 2002, one period in 2003, and during two periods in 2004. The focus is on the data collected in 2003 and 2004, and most of the next section will be devoted to the analysis of these data, which is slightly different from the analysis of the 2002 data (already published), thanks to various improvements in the analysis code. The new chain of analysis has also been used to reanalyse the 2002 data: the results are perfectly compatible, as will be shown in Section 6.1. Also, the new 2003–2004 data are in excellent agreement with the 2002 data. At the end, overall results will be given for the whole data set, 2002–2004.

## 3 Data analysis I - event reconstruction and selection
## 3.1 Event reconstruction

In the event reconstruction, a track reconstructed before the target is assumed to be an incoming muon if it is reconstructed in the scintillating fibres and silicons upstream of the target, its momentum is reconstructed in the BMS, and the track time is within 3 standard deviations

of BMS and trigger time. If several valid BMS-tracks are compatible with the track time, a backtracking algorithm is used to resolve ambiguities.

The scattered muon candidates are defined as the positively charged outgoing tracks with a momentum larger than 1 GeV/$c$, going through SM1, and their extrapolation at the entrance and at the exit of the target is within 5 cm from the target axis. In addition, for all triggers based on the hodoscope information, the track must be compatible with the hodoscope hits as given in the trigger matrix. In the case of a calorimetric trigger, a minimal number of hits is required in the muon walls and the amount of material traversed in the spectrometer must be larger than 66 and 74 radiation lengths for tracks reconstructed in the first and in the second spectrometer stage respectively.

The muon interaction point (the so-called "primary vertex") is defined by one beam particle and one scattered muon. If in the event there are more than one beam particles and/or scattered muons, several vertexes may be reconstructed. The distance of closest approach between the scattered muon and beam track must be less than 10 $\sigma$ (about 2–3 mm). The position of the vertex along the spectrometer axis $z_{vtx}$ [1] is given by the average of the distance of closest approach of all tracks in the vertex, while in the orthogonal plane the coordinates $x_{vtx}$ and $y_{vtx}$ are defined from the beam track at $z_{vtx}$. The tracks belonging to the vertex are selected using a Kalman fit. The "best primary vertex", used in the following steps of the analysis, is defined as the one with the maximum number of tracks and, if the number of tracks is the same, the one with smaller vertex $\chi^2$.

Only the events with at least one primary vertex reconstructed with at least one more outgoing track, and $Q^2 > 1$ (GeV/$c$)$^2$, which are about 1% of the initial raw event sample, are written on miniDST and used in the physics analysis.

The event reconstruction was almost the same for the 2003 and 2004 data, and is very similar to that used for the 2002 data. Each year an improvement in the ratio of reconstructed events over the useful beam was achieved, due both to additional detectors in the spectrometer and to the better tuned reconstruction and analysis software.

### 3.2 Data quality checks

To monitor the performances of the apparatus before and after the target spin reversal (i.e. on the two "sub-periods") in each data taking period, the time stability of many distributions has been checked dividing the whole sample into runs or clusters of neighbouring runs.

Using the histograms produced during the event reconstruction, the detector performance stabilities were scrutinised looking at the stability of the shape of the hit distributions in the about 360 detector planes. The time stability of the detector and reconstruction efficiencies was checked looking at:
- the number of clusters per plane and per event,
- the mean number of tracks per event,
- the mean number of track segments in the different spectrometer regions per event,
- the mean number of primary vertexes per event,
- the mean number of secondary vertexes per event.
Using the miniDST events, the stability was checked monitoring run per run
- the number of reconstructed $K^0$ per primary vertex,
- the reconstructed $K^0$ mass distribution,
- the energy measured in the two hadronic calorimeters $HCAL1$ and $HCAL2$,

---

[1] the used reference system is defined to have a right handed frame with the z axis along the spectrometer axis (i.e. the nominal beam direction) the y axis in the vertical direction pointing upwards, and the origin at the centre of the $u$-cell.
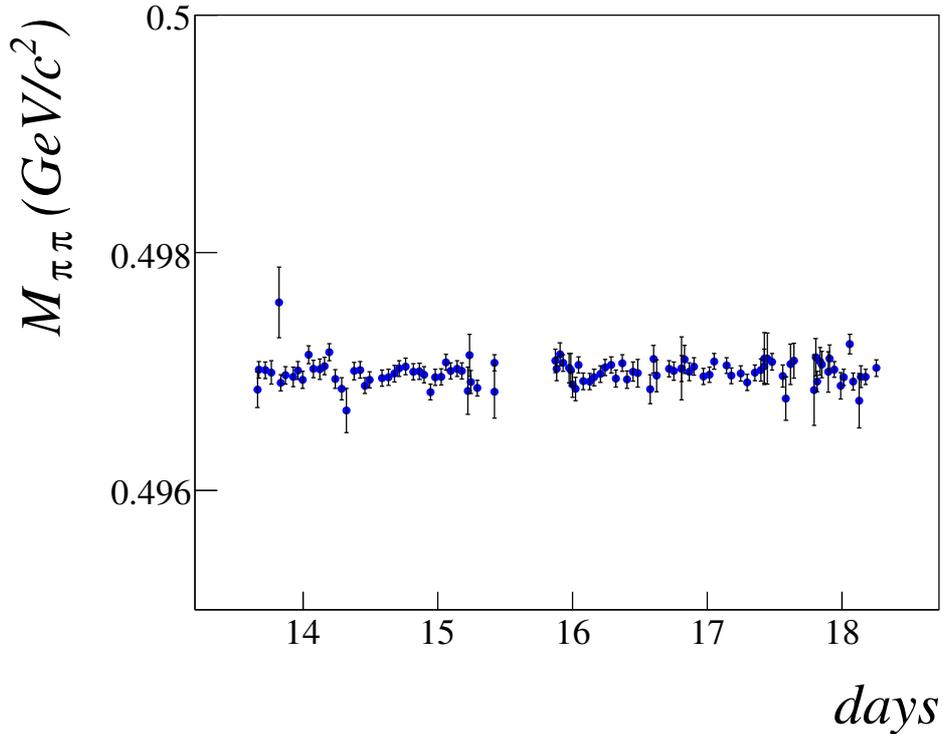
Figure 5: $\pi\pi$ invariant mass in the $K^0$ region as a function of time from August 13 to August 19, 2004.

- the $x_{vtx}$ and $y_{vtx}$ distributions in the two cells,
- the vertex $\chi^2$ distribution.

Also, the time stability of the distributions of several kinematical observables (like $x$, $Q^2$, $y$, the azimuthal angles and the momenta of the scattered muon and of the hadrons) was investigated in detail.

As an example, the mean $\pi\pi$ invariant mass in the $K^0$ region from the data collected in the first sub-period of the 2004 run is shown in Fig. 5 as a function of time.

Runs showing some instability were not used for the physics analysis. The runs rejected by this criterion are 28 (over a total of 458) for the 2003 data, and 44 (over 462) for the 2004 data, corresponding to about 5% and 4% of the initial raw event sample.

### 3.3 DIS events selection

To better define the DIS events, more refined cuts were applied. In particular:

1. primary vertex: if more primary vertexes were reconstructed in one event, the best primary vertex was selected.

   The vertex had then to be inside the target. A radial cut $r_{vtx} < 1.3$ cm was applied on the distance of the vertex from the target axis. The event was then accepted only if $z_{vtx}$ was inside one of the two target cells (-100 cm $< z_{vtx} <$ -40 cm or -30 cm $< z_{vtx} <$ 30 cm), and assigned correspondingly to the $u$- or to the $d$-cell.

   The distribution of the primary vertex z-coordinate for the final sample is shown in Fig. 6. The increase in the number of events with $z_{vtx}$ is due to the increase in geometrical acceptance going from the upstream to the downstream end of the target, as explained in Section 2.2, and is very well reproduced by the Monte Carlo simulation. The two target
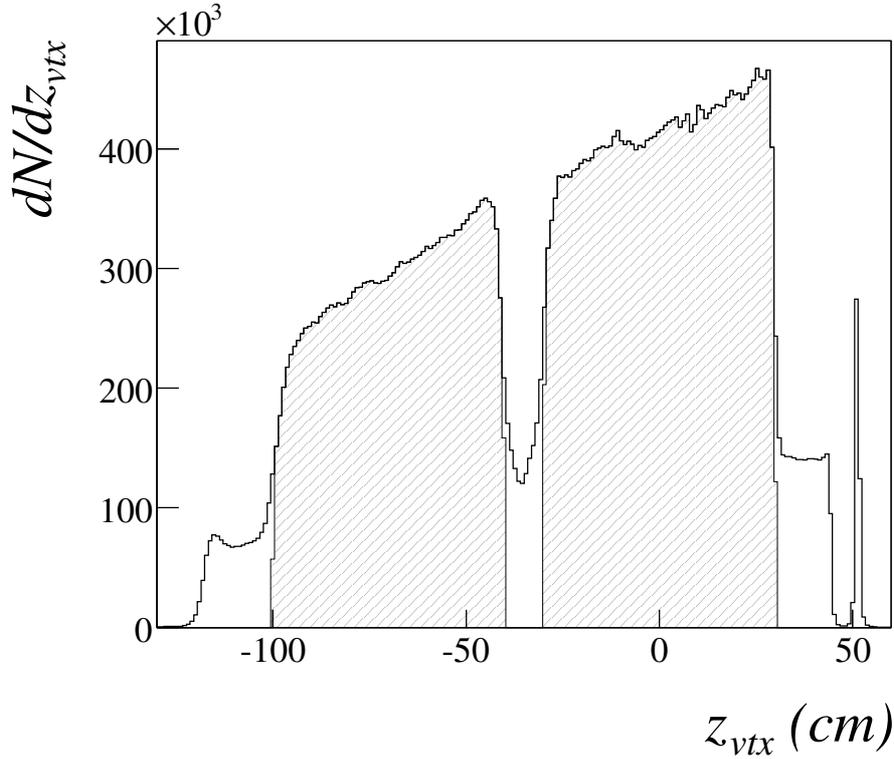
13

Figure 6: Distribution of the primary vertex z-coordinate for the final sample. The dashed histogram indicates the events selected by the $z_{vtx}$ cut.

    cells are clearly separated. One can also notice the continuum of events produced on the helium bath, as well as a sample of events produced in the Al window, at z= 50 cm, which seals the vessel of the PT magnet.

2. incoming muon: the cut $p_{beam} < 200$ GeV/$c$ was applied on the momentum of the incoming particle. A check was also performed on the quality of the beam track, and a safe cut on $\chi^2/\nu$ was applied.
   To ensure an identical beam intensity in both target cells, i.e. a nearly identical luminosity, the beam track projection at the entrance and at the exit of the target region (e.g. at z= −100 cm and z= 30 cm) had to be inside the target region as defined for the primary vertex. The momentum distribution for the final data sample is shown in Fig. 7.

3. scattered muon ($\mu'$): as well as for the incident muon, a suitable cut was applied on the $\chi^2/\nu$ of all reconstructed tracks from the vertex, including the scattered muon candidate. Other outgoing tracks were flagged as muon candidate if they had hits in one of the two Muon Walls. To achieve a clean muon identification, the amount of material traversed in the spectrometer had to be larger than 30 radiation lengths. Only events with one and only one muon candidate entered the following steps of the analysis.

In addition, standard DIS cuts $Q^2 > 1$ (GeV/$c$)$^2$, mass of the final hadronic state $W > 5$ GeV/$c^2$, and $0.1 < y < 0.9$ were applied. All these cuts reduced the number of miniDST events by a further 45%.

## 3.4   Hadron identification

    All the outgoing particles not flagged as $\mu'$ candidates were assumed to be hadrons.
    Only particles with the last measured coordinate after the first spectrometer magnet were
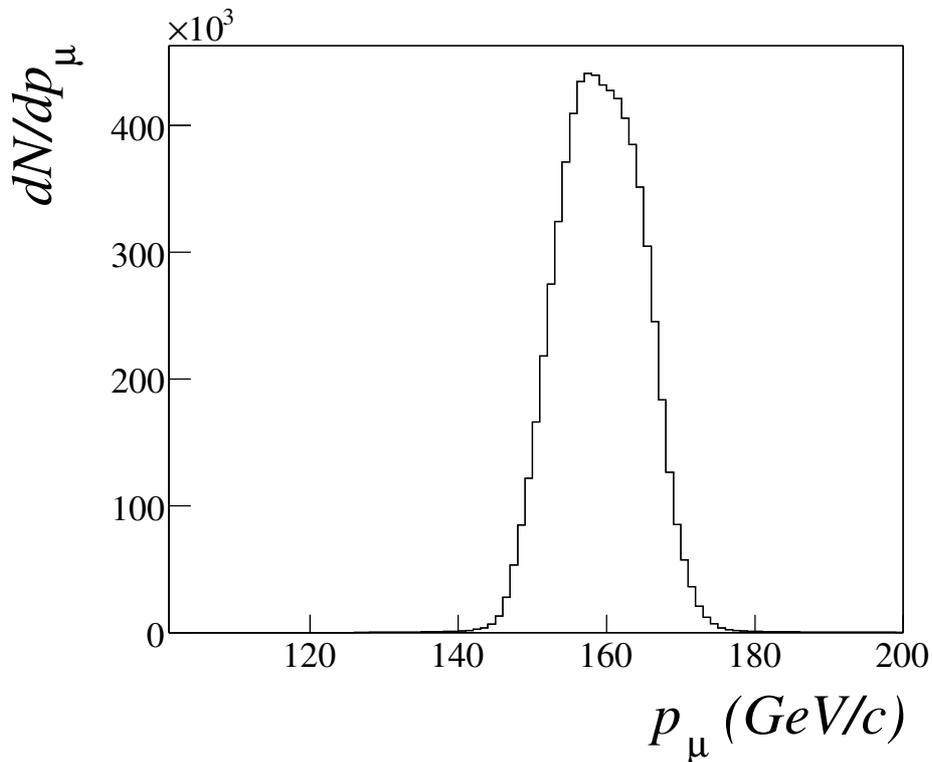
14

Figure 7: Momentum distribution of the reconstructed incoming muons for the final sample of events.

used, to reject tracks reconstructed in the fringe field on SM1 which have a poorer momentum resolution.

The following requirements had to be satisfied in order to identify the particle with a hadron:

1. the amount of material traversed in the spectrometer had to be smaller than 10 radiation lengths;

2. the particle must not give a signal in any of the two hadronic calorimeters $HCAL1$ and $HCAL2$.

3. if the particle gave a signal in one calorimeter, the measured energy had to be $E_{HCAL1} >$ 5 (2003 data) or 4 (2004 data) GeV, or $E_{HCAL2} > 5$ (2003 and 2004 data) GeV. The correlation between the energy measured in HCAL and that measured by the spectrometer is shown in Fig. 8.

4. the transverse momentum of the particle with respect to the virtual photon direction had to be larger than 0.1 GeV/$c$.

   The first requirement reduced the muon contamination, the second and the third the muon and the electron contamination. The last cut was introduced to assure a good resolution in the measured azimuthal angle.

Two different asymmetries have been measured. The "all hadron" asymmetries were evaluated using all the particles identified as hadrons carrying a fraction of available energy $z > 0.2$. For the "leading hadron" analysis, only the events with at least one hadron with $z > 0.25$ were used, and the hadron with largest $z$ was defined as leading. In the case the energy of the reconstructed leading hadron was higher than the missing energy evaluated from all the charged reconstructed hadrons, no further test was performed. If this was not the case, the event was accepted only
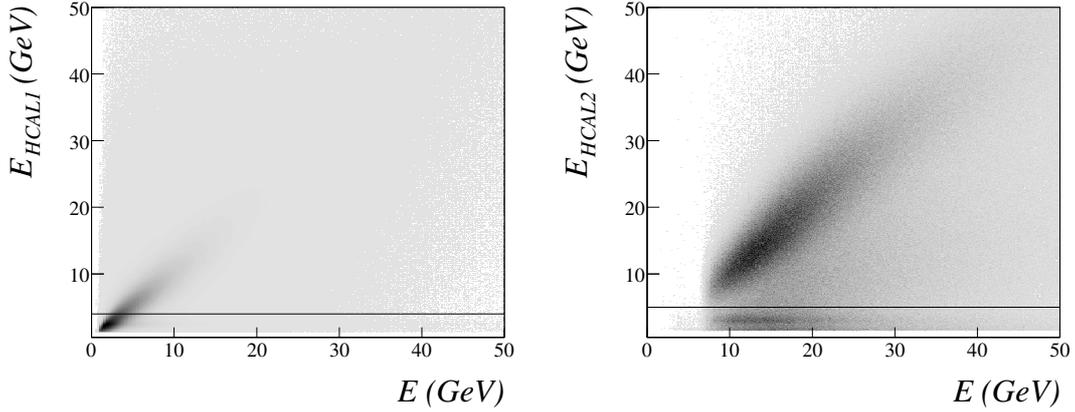
15

Figure 8: Correlation between the energy measured in HCAL1 (left) and HCAL2 (right) and the energy measured by the spectrometer for the 2004 data.

if in the hadron calorimeters no particle with energy larger (within the energy resolution) than that of the leading hadron was detected.

After these cuts, the number of events with a leading hadron amounted to 22% of the number of miniDST events.

## 4    Data analysis II - kinematical distributions and asymmetry evaluation
### 4.1    Final samples of events

In table 1, the final statistics used for the asymmetry evaluation is given for all the periods both for the positively and negatively charged "leading hadron" and the "all hadron" sample.

Table 1: Final statistics used for the asymmetry evaluation

| Year | Period | Leading hadron sample | | All hadron sample | |
|------|--------|-----------------|-----------------|-----------------|-----------------|
|      |        | positive hadrons | negative hadrons | positive hadrons | negative hadrons |
| 2002 | 1 | $0.48 \cdot 10^6$ | $0.38 \cdot 10^6$ | $0.71 \cdot 10^6$ | $0.59 \cdot 10^6$ |
| 2002 | 2 | $0.32 \cdot 10^6$ | $0.26 \cdot 10^6$ | $0.48 \cdot 10^6$ | $0.40 \cdot 10^6$ |
| 2003 | 1 | $1.68 \cdot 10^6$ | $1.33 \cdot 10^6$ | $2.46 \cdot 10^6$ | $2.03 \cdot 10^6$ |
| 2004 | 1 | $1.44 \cdot 10^6$ | $1.13 \cdot 10^6$ | $2.12 \cdot 10^6$ | $1.74 \cdot 10^6$ |
| 2004 | 2 | $1.87 \cdot 10^6$ | $1.47 \cdot 10^6$ | $2.75 \cdot 10^6$ | $2.26 \cdot 10^6$ |

### 4.2    Kinematical distributions

The distributions of some kinematical quantities from the final 2004 leading hadron events are shown in Figs. 9 to 11. The plots have been produced after all the cuts described in the previous section, if not specified differently.

The $Q^2$ vs $x$ scatter-plot and its projections are shown in Fig. 9.

The $x$-$z$ correlation (without the $z$ cut), the $x$-$y$ correlation, and the $z$-$p_T^h$ correlation (without the $z$ and the $p_T^h$ cuts) are shown in Fig. 10, while the $y$, $p_T^h$ (without the $p_T^h$ cut) and the $z$ (without the $z$ cut) distributions are shown in Fig. 11.
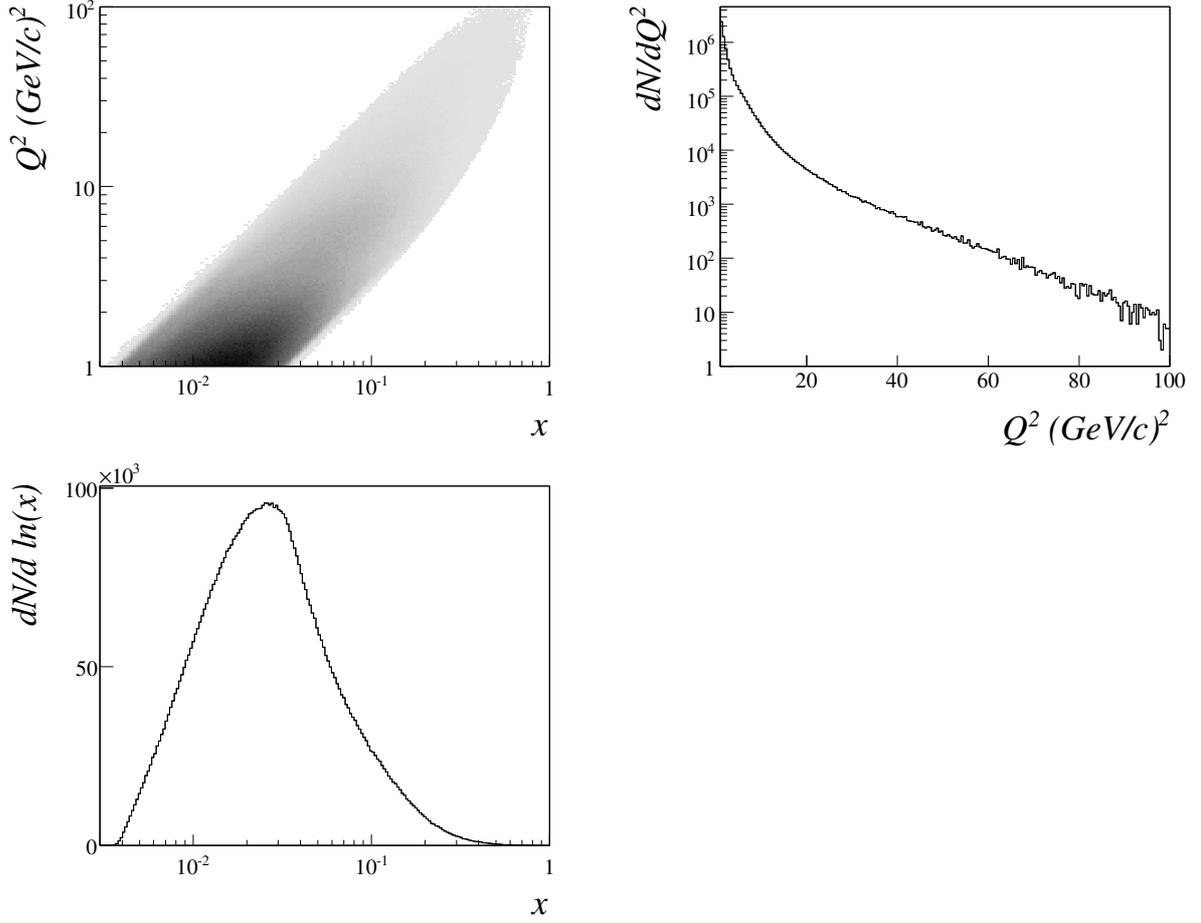
16

Figure 9: Scatter-plot of $Q^2$ vs $x$, and the corresponding $Q^2$- and $x$-distributions for the 2004 positive plus negative leading hadron sample.

### 4.3 Asymmetry evaluation

*4.3.1 Binning*

The Collins and Sivers asymmetries were evaluated as function of $x$, $p_T^h$, and $z$ dividing the corresponding kinematical range in bins (with variable width, in order to have a comparable statistics in each of them), and integrating over the other 2 variables. No attempt has been done to extract the asymmetries in a 2- or 3-dimensional grid. In total, the asymmetries where evaluated in the 9 $x$-bins, 9 $p_T^h$-bins, and 8 $z$-bins for the all hadron samples (7 for the leading hadron, because of the $z > 0.25$ cut) given in Table 2.

Tables with the mean values of $Q^2$, $z$, $p_T^h$ and $y$ in all the $x$ bins are available on HEP-DATA [41]. As an example, Fig. 12 shows the mean values of $Q^2$ (left), $z$, $p_T^h$ and $y$ (right) in the different $x$ bins for the all positive hadron sample from 2003 and 2004 data.

*4.3.2 Raw asymmetry evaluation*

The Collins and Sivers asymmetries have been evaluated separately, in each kinematic bin, for each data taking period, and for positive and negative hadrons.

Using Eq. (1) and (12), the $\Phi$ distribution of the number of events for each cell and for each polarisation state can be written as

$$N_{j,k}^{\pm}(\Phi_j) = F_k^{\pm}\, n_k\, \sigma \cdot a_{j,k}^{\pm}(\Phi_j) \cdot (1 \pm \epsilon_{j,k}^{\pm}\, \sin \Phi_j), \tag{18}$$
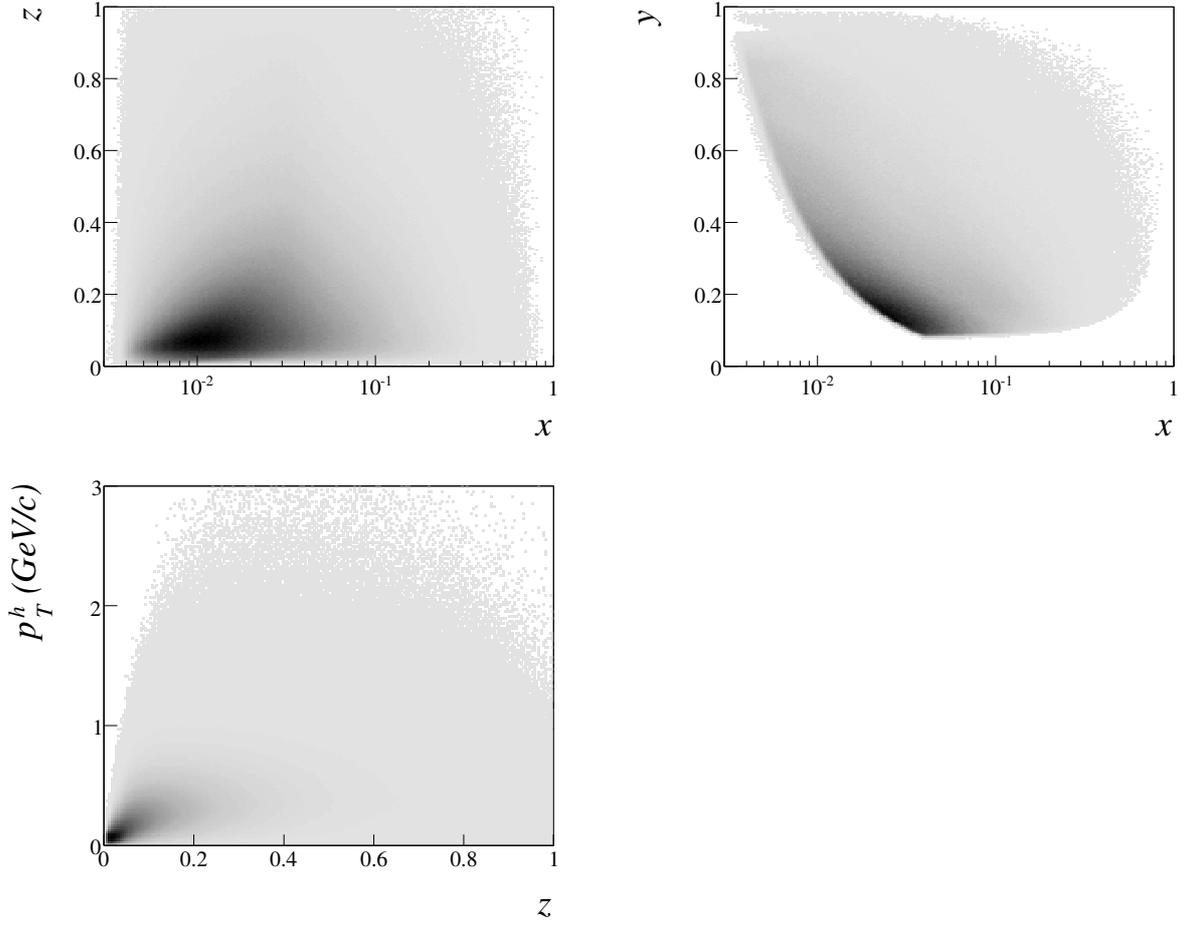
17

Figure 10: Scatter-plots of $z$ vs $x$, $y$ vs $x$, and $z$ vs $p_T^h$ for the 2004 all positive plus negative hadron samples.

where $j = C, S$, and $F$ is the muon flux, $n$ the number of target particles, $\sigma$ the spin averaged cross-section, and $a_j$ the product of angular acceptance and efficiency of the spectrometer. The index $k = u, d$ refers to the target cell. The $\pm$ signs indicate the two target spin orientations: $+$ means spin up, $-$ spin down. Here the Collins and Sivers angles $\Phi_j$ are evaluated using the expressions given in Sections 1.2 and 1.3, always assuming target spin up, at variance with what was done in [15].

| | | |
|---|---|---|
| $0.003 < x < 0.008$ | $0.20 \leq z < 0.25$ | $0.10 < p_T^h \leq 0.20$ GeV/$c$ |
| $0.008 \leq x < 0.013$ | $0.25 \leq z < 0.30$ | $0.20 < p_T^h \leq 0.30$ GeV/$c$ |
| $0.013 \leq x < 0.020$ | $0.30 \leq z < 0.35$ | $0.30 < p_T^h \leq 0.40$ GeV/$c$ |
| $0.020 \leq x < 0.032$ | $0.35 \leq z < 0.40$ | $0.40 < p_T^h \leq 0.50$ GeV/$c$ |
| $0.032 \leq x < 0.050$ | $0.40 \leq z < 0.50$ | $0.50 < p_T^h \leq 0.60$ GeV/$c$ |
| $0.050 \leq x < 0.080$ | $0.50 \leq z < 0.65$ | $0.60 < p_T^h \leq 0.75$ GeV/$c$ |
| $0.080 \leq x < 0.130$ | $0.65 \leq z < 0.80$ | $0.75 < p_T^h \leq 0.90$ GeV/$c$ |
| $0.130 \leq x < 0.210$ | $0.80 \leq z < 1.00$ | $0.90 < p_T^h \leq 1.30$ GeV/$c$ |
| $0.210 \leq x < 1.000$ | | $1.30 < p_T^h$ |

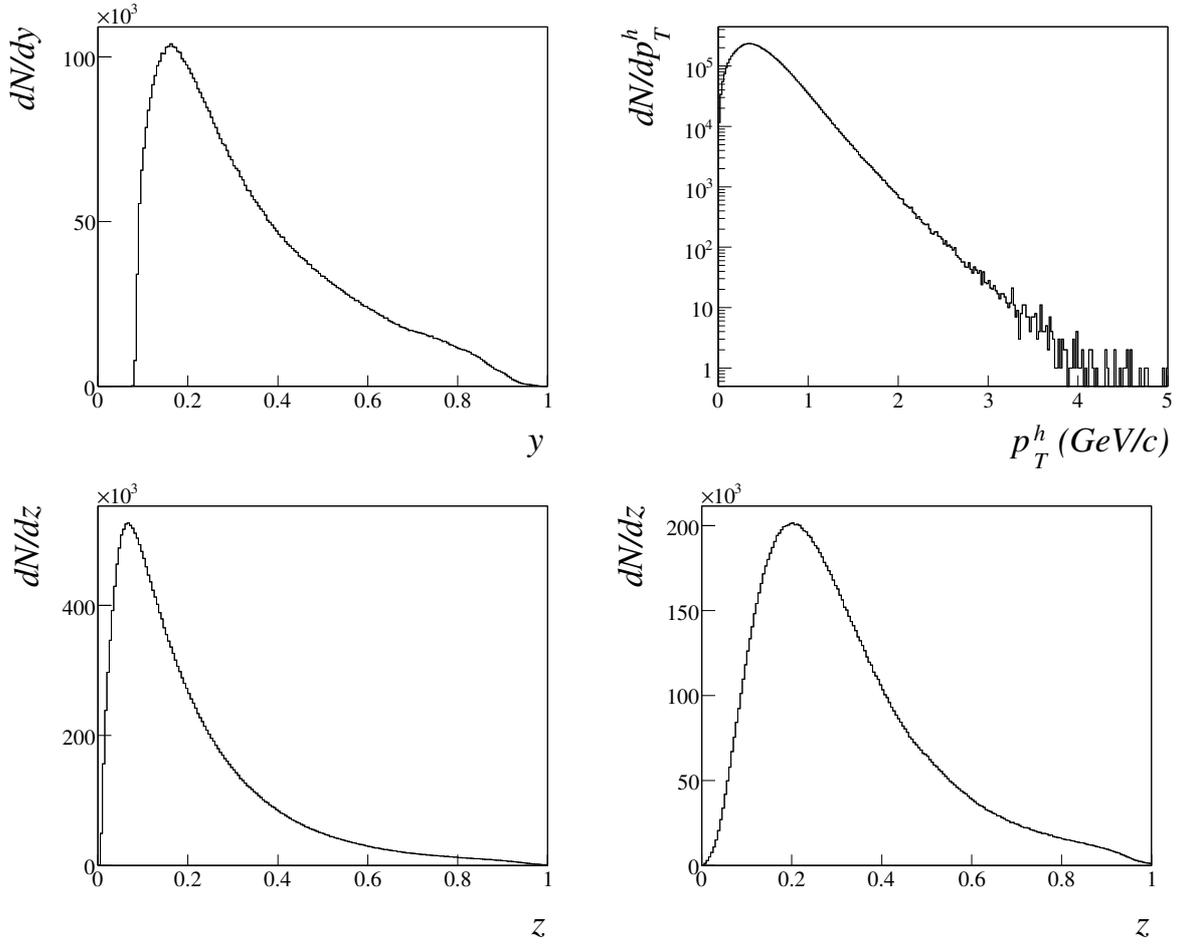Table 2: Final binning in $x$, $z$, and $p_T^h$.

Figure 11: Upper plots: distributions of $y$ and $p_T^h$ (without the $p_T^h$ cut) for the 2004 all positive plus negative hadron sample. Lower plots: $z$-distribution (without the $z$ cut) for the same events (left) and for the 2004 leading positive plus negative hadron sample (right).

The asymmetries $\epsilon_{j,k}^{\pm}$ are

$$\epsilon_{C,k}^{\pm} = c_{C,k}^{\pm} \cdot A_{Coll} , \quad \epsilon_{S,k}^{\pm} = c_{S,k}^{\pm} \cdot A_{Siv} , \tag{19}$$

where

$$c_{C,k}^{\pm} = f \cdot |P_{T,k}^{\pm}| \cdot D_{NN} , \quad c_{S,k}^{\pm} = f \cdot |P_{T,k}^{\pm}| . \tag{20}$$

The factor $f$ is the polarised target dilution factor, $P_{T,k}^{\pm}$ the deuteron polarisation, and $D_{NN}$ the transverse spin transfer coefficient from the initial to the struck quark given in Eq. (8). The absolute values of the target polarisation $P_T$ in the two cells and for the two spin orientations in the same cells differed up to about 7%.

In order to estimate $\epsilon_{j,k}^{\pm}$ from the measured number of events a method, which in the following will be called "ratio product method" (RPM), has been used which minimises the effect on the estimated asymmetries of possible acceptance variations.

In each data taking period, the "ratio product" quantities [15]

$$A_j(\Phi_j) = \frac{N_{j,u}^+(\Phi_j)}{N_{j,u}^-(\Phi_j)} \cdot \frac{N_{j,d}^+(\Phi_j)}{N_{j,d}^-(\Phi_j)}, \quad j = C, S \tag{21}$$
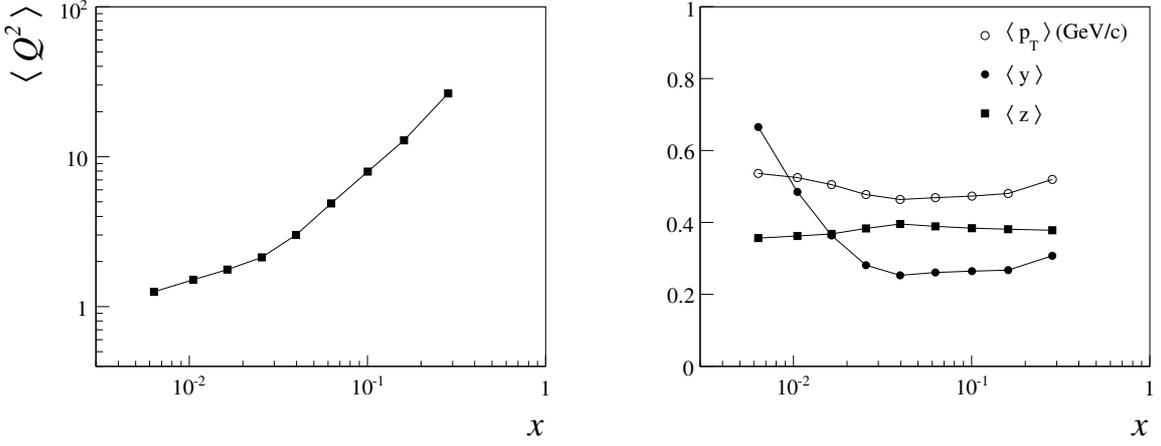
19

Figure 12: Mean values of $Q^2$ (left), $z$, $p_T^h$ and $y$ (right) in the different $x$ bins for all positive hadrons, 2003 and 2004 data.

were evaluated from the number of events in the two cells. For small values of the quantities $\epsilon_{j,k}^{\pm}$ it is:

$$
\begin{aligned}
A_j(\Phi_j) &= C_F \cdot C_{a,j} \cdot \frac{(1 + \epsilon_{j,u}^+ \cdot \sin \Phi_j) \cdot (1 + \epsilon_{j,d}^+ \cdot \sin \Phi_j)}{(1 - \epsilon_{j,u}^- \cdot \sin \Phi_j) \cdot (1 - \epsilon_{j,d}^- \cdot \sin \Phi_j)} \\
&\simeq C_F \cdot C_{a,j} \cdot (1 + A_j^m \cdot \sin \Phi_j)
\end{aligned}
\tag{22}
$$

where

$$
A_j^m = \epsilon_{j,u}^+ + \epsilon_{j,d}^+ + \epsilon_{j,u}^- + \epsilon_{j,d}^- = 4 \cdot < \epsilon_j >,
\tag{23}
$$

$$
C_F = \frac{F_u^+ \cdot F_d^+}{F_u^- \cdot F_d^-}, \quad C_{a,j} = \frac{a_{j,u}^+(\Phi_j) \cdot a_{j,d}^+(\Phi_j)}{a_{j,u}^-(\Phi_j) \cdot a_{j,d}^-(\Phi_j)}.
\tag{24}
$$

The raw asymmetries $A_C^m$ and $A_S^m$ were evaluated by fitting respectively the quantities $A_C(\Phi_C)$ and $A_S(\Phi_S)$ with the functions $p_0 \cdot (1 + A_C^m \cdot \sin \Phi_C)$ and $p_0 \cdot (1 + A_S^m \cdot \sin \Phi_S)$, where $p_0$ is a free parameter.

In this method the only requirement to avoid systematic errors due to acceptance effects is that the factor $C_{a,j}$ does not depend on $\Phi_j$. This is surely true, in particular, under the reasonable assumption that the ratio $a_{j,u}^+(\Phi_j)/ a_{j,d}^-(\Phi_j)$ before the polarisation reversal be equal to the corresponding ratio $a_{j,u}^-(\Phi_j)/ a_{j,d}^+(\Phi_j)$ after the reversal in each $\Phi_j$ bin. In this case, $C_{a,j}$ is equal to 1 for all $\Phi_j$ values. Also, with the cuts applied on the incoming beam it is expected that $C_F = 1$ and indeed the fits to $A_j^m$ give $p_0$ values always compatible with 1.

In addition to the fact that this estimator has "soft" requirements on the acceptance stability, it is independent of the relative luminosity and combines all the data from the two target cells. A further advantage of the use of the RPM, is that at first order (for small values of the involved asymmetries) all spin-independent effect, e.g. Cahn asymmetry, are factored out.

Concerning the $\Phi_j$ binning, the interval $(0, 2\pi)$ was divided in 16 bins. Monte Carlo studies indicated that the angular resolution (rms) is 0.07 rad, much smaller than the bin size.

### 4.3.3 Collins and Sivers asymmetries evaluation

To extract the Collins and Sivers asymmetries, the target polarisation values given in table 3 have been used.

20

| Year | Period/Subperiod | Polarisation | |
|------|------------------|--------------|---|
| | | upstream | downstream |
| 2003 | 1 / 1 | -49.7 | 52.8 |
| | 2 / 2 ($1^{st}$ part) | 49.4 | -42.6 |
| | 2 / 2 ($2^{nd}$ part) | 51.3 | -44.6 |
| 2004 | 1 / 1 | 50.70 | -43.52 |
| | 1 / 2 ($1^{st}$ part) | -44.8 | 46.0 |
| | 1 / 2 ($2^{nd}$ part) | -38.6 | 40.4 |
| | 2 / 1 ($1^{st}$ part) | -46.1 | 47.4 |
| | 2 / 1 ($2^{nd}$ part) | -46.4 | 47.4 |
| | 2 / 2 | 49.9 | -42.8 |

Table 3: Target polarisation values for the 2003 and 2004 data taking.

The dilution factor $f$ has been taken constant and equal to 0.38 for all data taking periods.

Using the event kinematics, the mean values of the quantities $c_{C,k}^{\pm} = f \cdot |P_{T,k}^{\pm}| \cdot D_{NN}$ and $c_{S,k}^{\pm} = f \cdot |P_{T,k}^{\pm}|$ have been evaluated for each bin and each period of data taking. These values have than been used to calculate the Collins and Sivers asymmetries from the corresponding raw asymmetries $A_j^m$.

# 5 Data analysis III - Systematic studies

Given the high statistics of our measurements, a number of systematic studies have been performed in order to determine the size of possible systematic errors.

Extensive tests both to measure false asymmetries and to investigate the stability of the physics results were done, for each measured asymmetry, and in each data taking period. They are briefly described in the following.

## 5.1 False asymmetry studies

Two different kinds of asymmetries expected to be zero were measured using the final event samples, for the Collins and Sivers angles, positive and negative hadrons, leading and all hadrons, and in each $x$, $z$, $p_T^h$ bin.

The first one was built by splitting the two target cells in two parts and by combining the data from the same cell. The mean values of all the resulting asymmetries were found to be compatible with zero, as it should. The distributions of the pulls of these asymmetries with respect to zero, i.e. the values of the resulting asymmetries divided by the corresponding standard deviation, were well compatible with Standard Normal distributions, giving no indication of the presence of systematic effects.

The second asymmetry was measured after scrambling the data collected in each period and measuring the asymmetry in the standard way. The runs of the two sub-periods before and after the polarisation reversal were mixed by labelling as "spin up" every 1st, 3rd, 5th, ... run of the two sub-periods and as "spin down" all the others. This selection was truncated in a way, that each fake period had the same amount of runs from each real sub-period to ensure roughly the same amount of events. As in the previous case, the asymmetries are expected to be zero, and the measured asymmetries were compatible with zero. The refined statistical analysis of pulls with respect to zero did not give any hint for the presence of systematic effects.

## 5.2 Stability of physics asymmetries vs acceptance and time

Possible acceptance effects on the physics results from each data taking period were tested by checking the compatibility of the asymmetries evaluated after splitting the data according to: the location inside the target; the region of the spectrometer in which the scattered muon was measured; the trigger of each event. This work was done for both the Collins and Sivers asymmetries of positive and negative hadrons, leading and all, and in each $x$, $z$, $p_T^h$ bin.

The compatibility test consisted in comparing the distribution of the pulls

$$P_{i,k} = \frac{A_{i,k}^m - A_k^m}{\sqrt{\sigma_{A_{i,k}^m}^2 - \sigma_{A_k^m}^2}} \qquad (25)$$

with the normal standard distribution. Here $A_k^m$ are the raw asymmetries evaluated from the whole data sample of one specific period $k$. They are evaluated for positive and negative hadrons, Collins and Sivers asymmetries in each $x$, $p_T^h$ and $z$ bin, for a total of $2 \times 2 \times (9 + 9 + 7) = 100$ values in each period. The corresponding variance is $\sigma_{A_k^m}^2$. The asymmetries $A_{i,k}^m$ are the corresponding ones evaluated for all the sub-samples $i$ in which the original data set was divided. The variances of $A_{i,k}^m$ are $\sigma_{A_{i,k}^m}^2$, and the use of the difference with $\sigma_{A_k^m}^2$ takes into account almost completely all the correlations between $A_{i,k}^m$ and $A_k^m$. The compatibility with the normal standard distribution was checked also for some specific group of asymmetries, like positive and negative hadrons, and Collins and Sivers asymmetries.

The effect of the different acceptances for events with the primary vertex in the two target cells was investigated, evaluating the physics asymmetries separately for the events with the primary vertex in the inner half and in the outer half of the two target cells. Combining events from only the outer halves (upstream part of cell $u$ and downstream part of cell $d$) as well as from the inner halves only (downstream part of cell $u$ and upstream part of cell $d$) gave results compatible to each other and to the ones using the full sample.

The asymmetries were also evaluated dividing the data samples accordingly to the azimuthal angle $\Phi_{\mu'}$ of the scattered muon in the laboratory system, namely in the regions $0 < \Phi_{\mu'} < \pi/2$, $\pi/2 < \Phi_{\mu'} < \pi$, $\pi < \Phi_{\mu'} < 3\pi/2$, and $3\pi/2 < \Phi_{\mu'} < 2p$.

As in the previous case, the pull distributions turned out to be centred around zero, and in very good agreement with the standard distribution. The RMS were statistically compatible with 1, as expected in the absence of systematic effects.

The physics asymmetries have been evaluated splitting the data in different samples according to the different triggers. The results turned out to be statistically compatible, giving once more no evidence for systematic effect.

A further test was done to investigate the stability in time of the physics asymmetries. To do this, each of the two sub-periods entering the standard asymmetry calculation was split in these 9 groups of subsequent runs (each corresponding to $\approx 10$ hours of data taking). The asymmetries were then calculated using the full data set of one sub-period and all the 9 groups of runs of the other sub-period separately. In total 54 asymmetries were evaluated from the 2003 and 2004 data. This method is known to be quite powerful to single out significant time dependencies within single periods. As for the previous test, the pulls relative to the mean asymmetry for each time slot region were calculated, but no evidence for systematic errors was found in their distributions.

A further test was done to check the possible effect of $z$ and $p_T^h$ acceptance. The asymmetries were evaluated also in 4 complementary $z$ and $p_T^h$ bins: ($z < 0.5$, $p_T^h < 0.5$), ($z < 0.5$, $p_T^h > 0.5$), ($z > 0.5$, $p_T^h < 0.5$), ($z > 0.5$, $p_T^h > 0.5$) and their weighted means were compared with the standard results. The differences between the two sets of measurements are essen-

tially invisible, much much smaller than the statistical errors, again as expected in absence of systematic effects.

## 5.3 Stability of the acceptance in the Collins and Sivers angles

A stringent test on the $\Phi_j$ ($j = C, s$) dependence of the acceptance ratio, already used for the previously published data, consists in checking the $\Phi_j$ dependence of the ratios:

$$R_j(\Phi_j) \;\;=\;\; \frac{N_{j,u}^+(\Phi_j) \cdot N_{j,d}^-(\Phi_j)}{N_{j,u}^-(\Phi_j) \cdot N_{j,d}^+(\Phi_j)} \tag{26}$$

At the first order, assuming the absolute value of the target polarisation to be the same in each cell before and after reversal, it is

$$R_j(\Phi_j) \;\;\simeq\;\; \frac{F_u^+ \cdot F_d^-}{F_u^- \cdot F_d^+} \cdot \frac{a_{j,u}^+(\Phi_j) \cdot a_{j,d}^-(\Phi_j)}{a_{j,u}^-(\Phi_j) \cdot a_{j,d}^+(\Phi_j)} \cdot \tag{27}$$

In the very likely case in which $a_{j,u}^+(\Phi_j)/a_{j,d}^-(\Phi_j) = a_{j,u}^-(\Phi_j)/a_{j,d}^+(\Phi_j)$ it is

$$R_j(\Phi_j) \;\;\simeq\;\; \frac{F_u^+ \cdot F_d^-}{F_u^- \cdot F_d^+} \cdot \left( \frac{a_{j,u}^+(\Phi_j)}{a_{j,u}^-(\Phi_j)} \right)^2$$

$$\;\;\simeq\;\; \frac{F_u^+ \cdot F_d^-}{F_u^- \cdot F_d^+} \cdot \left( \frac{a_{j,d}^-(\Phi_j)}{a_{j,d}^+(\Phi_j)} \right)^2 , \tag{28}$$

thus, the constancy in $\Phi_j$ of $R_j(\Phi_j)$ implies for each cell the ratio of the acceptances before and after the reversal to be constant in $\Phi_j$. It must be noted that this constancy is not required to have unbiased estimators in the case the asymmetries are evaluated with the RPM. Still, this test is quite convincing on the stability of the apparatus.

The ratios $R_j$ were calculated in each bin of $x$, $z$, $p_T^h$, for the Collins and Sivers angles, for leading and all hadrons and for both charges. In each bin the $\Phi_j$ distribution was fitted with a constant. Fig. 13 shows an example of the $R_C$ values for the Collins leading hadron sample in the 9 $x$-bins for the first period of data taking in 2004. The lines are the results of the fit. The quality of these fits are very good, as can be seen from Fig. 14 where the distribution of the $\chi^2$ of all the fits is compared with the expected $\chi^2$ distribution for $\nu = 15$ degrees of freedom normalised to the number of entries. To conclude, this test gave an independent indication on the stability of the acceptances.

Summarising, all the test we performed on the effects of acceptance and on fluctuation in time of the measured asymmetries gave results statistically compatible with what expected in the absence of systematic effects.

## 5.4 Further tests on the fit of the ratio product quantities

The quality of the fit of the double ratio quantities $A_j^m$ with the function $p_0 \cdot (1. + A_j^m \cdot \sin \Phi_j)$ has been checked looking at the $\chi^2$ distribution. Fig. 15 shows the $\chi^2$ distribution for Collins and Sivers asymmetries, in each bin of $x$, $z$, $p_T^h$ for leading hadrons of both charges and for all the 5 data taking periods in 2002, 2003, and 2004. The curve is the expected $\chi^2$ distribution for 14 degrees of freedom normalised to the number of entries. A perfect agreement can be observed.

The effect of using two other different fitting functions, namely $(1 + A_{m,j} \cdot \sin \Phi_j)$ and $(p_0 + A_{m,j} \cdot \sin \Phi_j)$, as well as changing the $\Phi_j$ bin size (8 bins instead of 16) have also been investigated. In both cases the effects turned out to be negligible, of the order of a few percents of the statistical error.
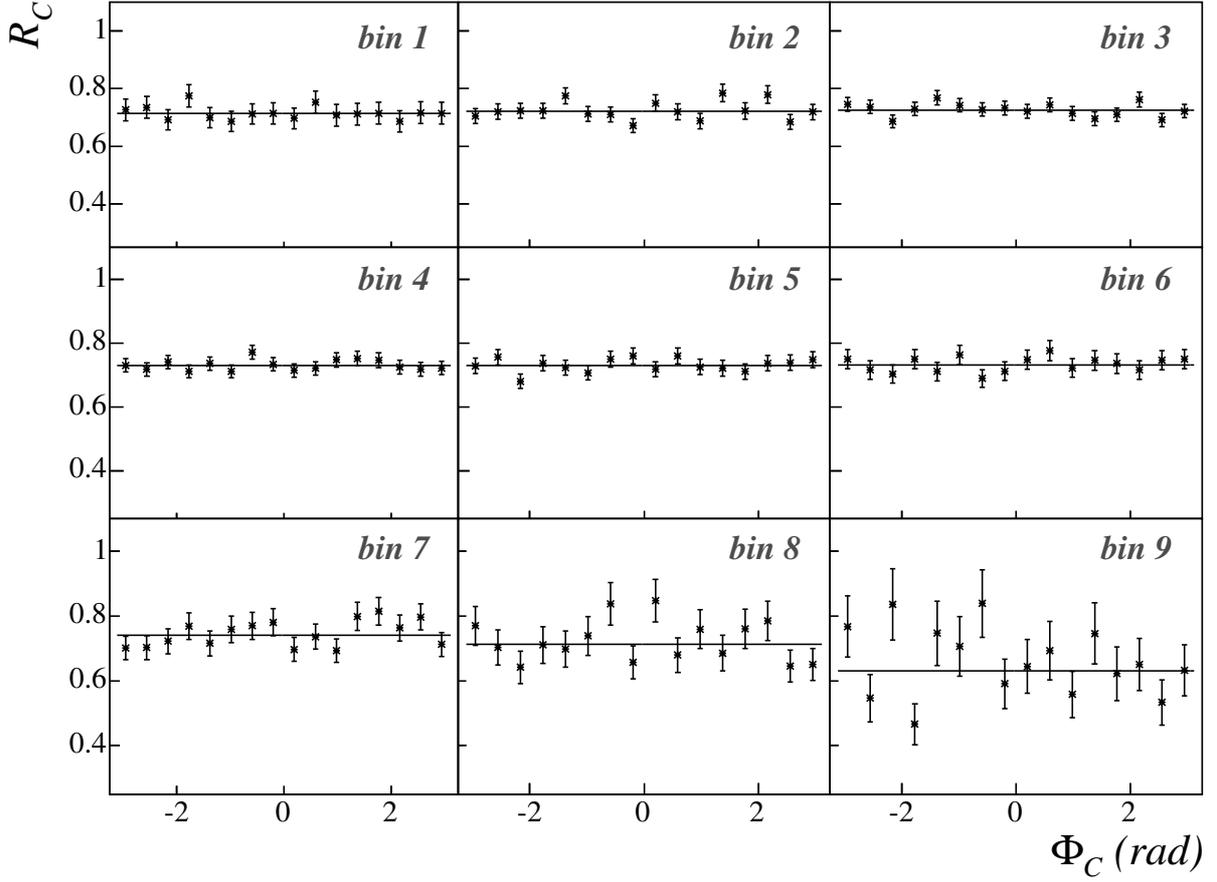
Figure 13: Distribution of the $R_C$ values for the Collins leading hadron sample vs. $x$ for the first period of data taking in 2004. The line shows the result the fit with a constant value.

## 5.5   Different estimators

To estimate the size of possible systematic effects, the asymmetries have also been evaluated using two other estimators which rely on different assumptions of the acceptance variations, namely the "difference method" (DM, in the following) and the "geometric mean method" (GMM), which are commonly used in evaluating asymmetries.

The DM was used to extract the final values of the asymmetries published in [15]. The evaluation of the asymmetries is performed separately for the two target cells and, after checking their compatibility, they are combined by taking weighted averages. The asymmetries $\epsilon_{C,k}$ and $\epsilon_{S,k}$, where $k = u, d$ indicates the target cell, were evaluated from the number of events with the two target spin orientations (+ spin up, and - spin down) by fitting the quantities

$$D_{j,k}^m(\Phi_j) = \frac{N_{j,k}^+(\Phi_j) - r_k \cdot N_{j,k}^-(\Phi_j)}{N_{j,k}^+(\Phi_j) + r_k \cdot N_{j,k}^-(\Phi_j)} , \quad j = C, S \tag{29}$$

with the functions $\epsilon_{C,k} \cdot \sin \Phi_C$ and $\epsilon_{S,k} \cdot \sin \Phi_S$. The normalisation factor $r_k$ was taken equal to the ratio of the total number of detected events in the two orientations of the target polarisation: $r = N_{h,tot,k}^+/N_{h,tot,k}^-$. This procedure is correct if the difference of the absolute value of the target polarisation before and after the spin reversal is negligible. For what concerns the acceptances, they cancel in Eq. (29) as long as the ratio $a_{j,k}^+(\Phi_j)/a_{j,k}^-(\Phi_j)$ is constant in $\Phi_j$.

In the GMM, again the asymmetries are evaluated separately for the two target cells and then combined by taking weighted averages. The method consists in building the measured
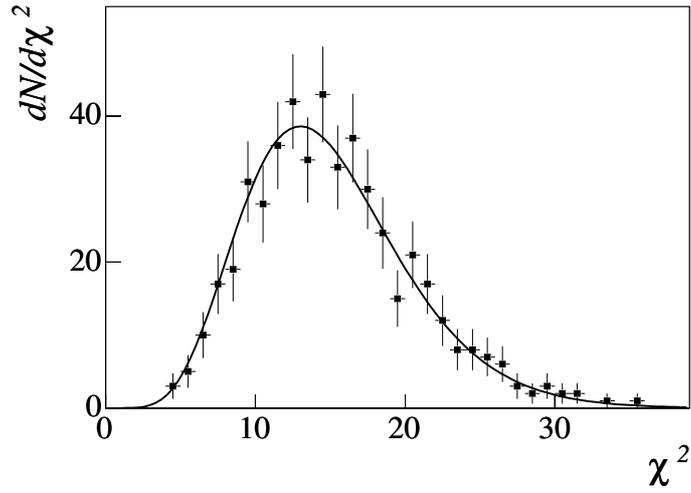
Figure 14: The $\chi^2$ distribution of a constant fit on $R(\Phi)$ for the leading hadron sample compared to the normalised $\chi^2$ distribution for $ndf = 15$.

quantities

$$G_{j,k}^m(\Phi_j) = \frac{\sqrt{N_{j,k}^+(\Phi_j) \cdot N_{j,k}^-(\Phi_j + \pi)} - \sqrt{N_{j,k}^-(\Phi_j) \cdot N_{j,k}^+(\Phi_j + \pi)}}{\sqrt{N_{j,k}^+(\Phi_j) \cdot N_{j,k}^-(\Phi_j + \pi)} + \sqrt{N_{j,k}^-(\Phi_j) \cdot N_{j,k}^+(\Phi_j + \pi)}}.$$

(30)

Assuming:
- a negligible difference in the absolute value of the target polarisation before and after the spin reversal (as for the DM), and
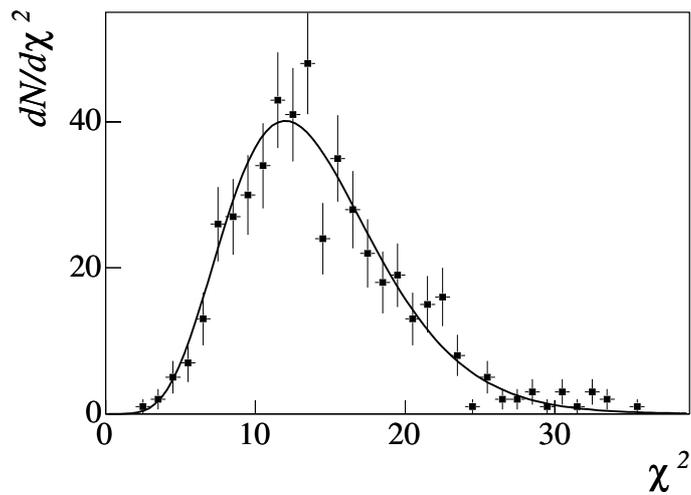


Figure 15: $\chi^2$ distribution of the two parameter fit used to extract the asymmetries $A_j^m$ compared to the normalised $\chi^2$ distribution for $ndf = 14$.

25

- that the acceptances satisfy the relation

$$\frac{a_{j,k}^+(\Phi_j)}{a_{j,k}^+(\Phi_j + \pi)} = \frac{a_{j,k}^-(\Phi_j)}{a_{j,k}^-(\Phi_j + \pi)} \tag{31}$$

the asymmetries are evaluated by fitting the quantities $G_{j,k}^m(\Phi_j)$ with the functions $\epsilon_{C,k} \cdot \sin \Phi_C$ and $\epsilon_{S,k} \cdot \sin \Phi_S$ in the range $0 \leq \Phi_{C,S} < \pi$.

The advantage of this method is that the luminosity cancels. Still, the requirement on the acceptance stability is more demanding than in the case of the ratio product method, which was thus used to evaluate the final asymmetries.

The fitted asymmetry values from the three methods were very close. Given the advantages of the RPM, the evaluation of the asymmetries with the GMM and DM has been considered only a cross-check of the result, and the results of the experiment given in the following are those obtained using the RPM method.

### 5.6 2-D fits

In an entirely different approach, we have estimated the Collins and Sivers asymmetries using the standard linear least square method (LSM) and fitted in each kinematics bin the measured asymmetries

$$A_j(\phi_h, \phi_S) = \frac{N_{j,u}^+(\phi_h, \phi_S)}{N_{j,u}^-(\phi_h, \phi_S)} \cdot \frac{N_{j,d}^+(\phi_h, \phi_S)}{N_{j,d}^-(\phi_h, \phi_S)} \tag{32}$$

with the function

$$\begin{aligned} H(\phi_h, \phi_S) &= a_1 + a_2 \sin(\phi_h + \phi_S - \pi) + a_3 \sin(3\phi_h - \phi_S) + \\ &\quad + a_4 \sin(\phi_h - \phi_S) + a_5 \cos(\phi_h - \phi_S) . \end{aligned} \tag{33}$$

The first parameter should be one. The second, third and fourth terms arise from the transverse component of the target nucleon spin when the lepton beam is unpolarised, while the last term originates from the interaction between a longitudinally polarised lepton beam and a transversely polarised target (see ref [42]). The second term is the Collins term. The fourth term is the Sivers term. The last term has also physics interest of its own, it is related to the $g_{1T}$ transverse momentum distribution function.

In order to have enough statistics in each $(\phi_h, \phi_S)$ bin, we have plotted the data in 8 bins of $\phi_h$ and 8 bins of $\phi_S$. Each kinematic bin is thus split in 64 $(\phi_h, \phi_S)$ bins. We have performed both 5-parameter fits and 4-parameter fits, in this second case fixing a1 to its expected value of 1. Also, we have done two independent fits, one minimising a $\chi^2$ with a linear LSM, the second using MINUIT [43]. The results of the four fits are in excellent agreement, and both the fitted Collins and Sivers asymmetries and their errors turn out to be essentially identical to the values given by the one dimensional fits, as expected from the orthogonality of the different terms. The Collins and Sivers asymmetries as given by the 2-D fit turn out to be slightly correlated (the correlation coefficient ranges from -0.25 to 0.25), a known effect due to the considerably non uniform population of the 64 $(\phi_h, \phi_S)$ bins.

A full discussion of the procedure and of the results will be the subject of a separate paper.

### 5.7 Systematic errors

As spelled out in the previous sections, all tests performed in the different data taking periods did not give any evidence for the presence of systematic effects.
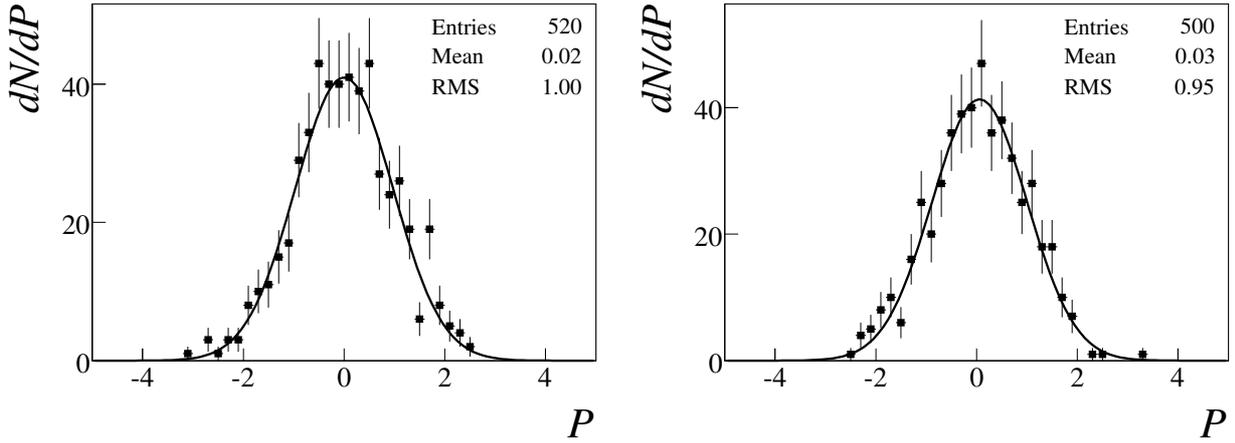
26

Figure 16: Distributions of $P_{k,j}$ (see text) for the leading hadron (left) and all hadron (right) asymmetries.

The conclusive test was to look at the compatibility of the physics results obtained separately for all the data taking periods. As already mentioned, from 2002 to 2004 data were collected in 5 periods and the compatibility test is significant. It has to be stressed that the 2002 data from which the results have already been published, have been reanalysed using the slightly different event selection and analysis described here. The published data turned out to be very close to the new ones, with differences of the order of half of the systematic errors only in the less populated bins, essentially because of the different method used to evaluate the asymmetries (RPM instead of the DM used previously).

The test was performed separately for all hadron and leading hadrons asymmetries, following the procedure described in Section 5.2. The Collins and Sivers asymmetries in each $x$, $p_T^h$ and $z$ bin, for positive and negative hadrons, obtained in the 5 periods were compared with their weighted mean. The pulls are defined as

$$P_{k,j} = \frac{A_{k,j}^m - A_j^m}{\sqrt{\sigma_{A_{k,j}^m}^2 - \sigma_{A_j^m}^2}}, \quad k = 1, 5 \tag{34}$$

where $A_j^m$ are the weighted means of the asymmetries, and are expected to follow a normal standard distribution. In total there are 500 $P_{k,j}$ values for the leading hadron asymmetries and 520 for the all hadron asymmetries.

The distribution of the $P_{k,j}$ values for all hadrons and for leading hadrons are shown in figure 16. As expected, these pulls follow a normal distribution. A very good agreement with purely statistical fluctuations has been seen for all the various subsamples of the asymmetries; the RMS of the different distributions are given for completeness in table 4.

Since even in this last test we could not observe any indication for systematic effects, we concluded that the systematic errors due to acceptance and efficiency effects are considerably smaller than the statistical errors.

The asymmetry scale uncertainty due to the uncertainties on $P_T$ is of 5%. The error on the dilution factor $f$, which takes into account the uncertainty on the target composition, is of the order of 6%. When combined in quadrature, these errors give a global scale uncertainty of 8%.

Table 4: RMS of the pull distributions for the different samples of asymmetries

| Asymmetries | | | RMS | |
|---|---|---|---|---|
| positive hadrons | leading | Collins | 0.882 | ±0.056 |
| | | Sivers | 0.895 | ±0.057 |
| | all | Collins | 0.919 | ±0.057 |
| | | Sivers | 0.974 | ±0.060 |
| negative hadrons | leading | Collins | 1.043 | ±0.066 |
| | | Sivers | 0.971 | ±0.061 |
| | all | Collins | 1.092 | ±0.068 |
| | | Sivers | 0.991 | ±0.061 |
| leading | | | 0.950 | ±0.030 |
| all | | | 0.996 | ±0.031 |
| positive | | | 0.919 | ±0.029 |
| negative | | | 1.026 | ±0.032 |

## 6    Results and comparison with models

### 6.1    Measured asymmetries

The results from the different data taking periods have been combined by making the standard weighted mean.

Plots of the measured values of the Collins and Sivers asymmetries $A_{Coll}$ and $A_{Siv}$ for the 2003–2004 leading hadron sample against the three kinematic variables $x$, $z$ and $p_T^h$ are given in Fig. 17. Full points and open points refer to positive and negative hadrons respectively. The errors shown in the figure are only statistical. The same asymmetries are shown in Fig. 18 for the 2003–2004 all hadron sample. Again, the errors shown in the figure are only statistical.

The improvement in statistics with respect to the 2002 published result is clearly visible in Fig. 19, where, as an example, the published Collins asymmetry data for all positive (left) and all negative (right) hadrons are compared with the 2003–2004 results.

As already mentioned, the 2002 data have been reanalysed using the event selection and the analysis described in this paper. The effect on the measured asymmetries is very small, and is mainly due to use of the RPM in evaluating the raw asymmetries. As an example, Fig. 20 shows the comparison between the published and the new results for the Collins asymmetry. The new values from the 2002 data have been combined with the results from the 2003–2004 data to evaluate the final asymmetries.

The overall results from 2002–2004 deuteron target for the leading hadron sample and for the all hadron sample are given in Fig. 21 and 22 respectively. All these measured asymmetries are available on HEPDATA [41].

### 6.2    Comments and comparison with models

As apparent from Fig. 21 and 22, all the measured asymmetries are small, if any, and compatible with zero. This trend already characterised the published data of the 2002 run, and is confirmed by the new data with considerably improved precision. Small asymmetries is not a surprise. From the very beginning it was predicted that transverse spin effects be small in the deuteron due to the opposite sign which was expected for the $u$ and $d$ distributions, causing cancellations on the asymmetries of an isoscalar target, very much like in the helicity case. Still, it was not obvious that they would have been so small.

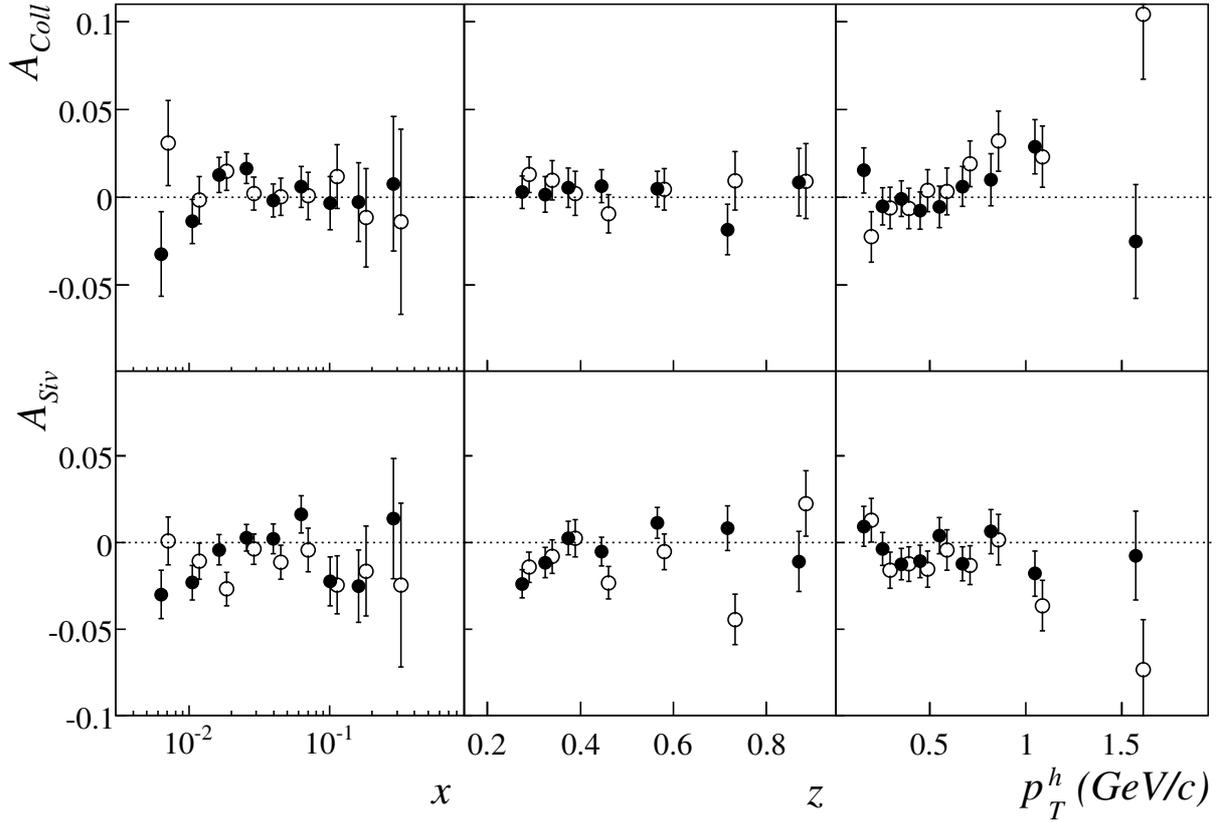An analysis of the results on the deuteron can be done only in conjunction with corre-

Figure 17: Collins asymmetry (top) and Sivers asymmetry (bottom) against $x$, $z$ and $p_T^h$ for positive (full circles) and negative leading hadrons (open circles) from 2003–2004 data. Error bars are statistical only. In all the plots the open circles are slightly shifted horizontally with respect to the measured value.

sponding proton data, which up to now have been measured only by the HERMES Collaboration [14]. The measured non zero Collins asymmetry on the proton has provided convincing evidence that both the transversity distribution $\Delta_T u(x)$ and the Collins mechanism $\Delta_T^0 D_u^h(z)$ are not zero. Independent evidence that the Collins mechanism is a real measurable effect has come from the recent analysis of the BELLE Collaboration [44,45]. Furthermore, the HERMES data on a proton target have provided convincing evidence that the Sivers mechanism is also at work.

It is fair to say that the accuracy of the present HERMES data has allowed to extract only the leading contribution to the proton transverse asymmetry, that is the u quark contribution. Also, the interpretation of the HERMES data has led to surprising assumptions about the relative size of the favoured and unfavoured spin dependent fragmentation functions. A global analysis using all the available deuteron and proton data should allow now to provide first estimates of both the u and the d quark contribution, and clearly constitutes the next step in this work.

In the following, first naive expectations, based on the simple formulas of Sections 1.2 and 1.3, are given for the deuteron asymmetries, then the new deuteron data are compared to a few existing model calculations.
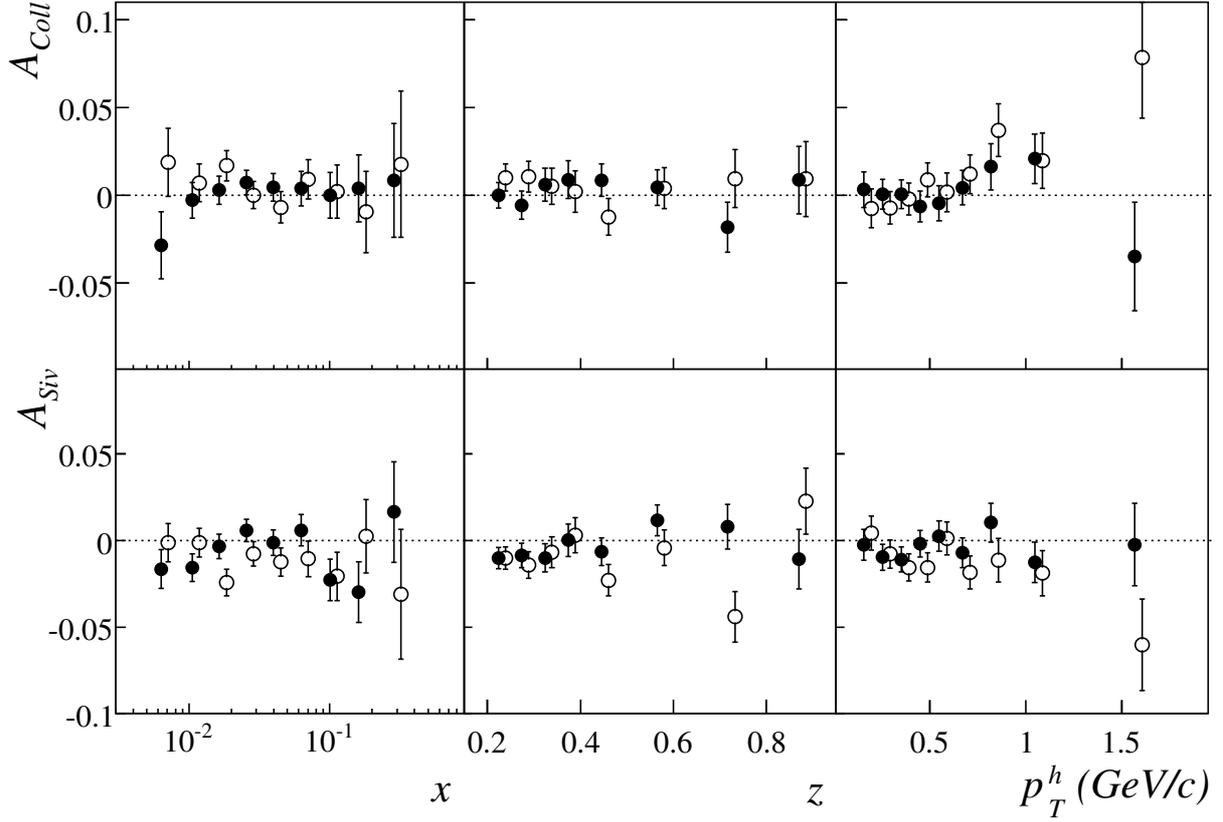
Figure 18: Collins asymmetry (top) and Sivers asymmetry (bottom) against $x$, $z$ and $p_T^h$ for positive (full circles) and negative hadrons (open circles) from 2003–2004 data. Error bars are statistical only. In all the plots the open circles are slightly shifted horizontally with respect to the measured value.

### 6.2.1 Collins asymmetry

Although the measured deuteron asymmetries refer to unidentified hadrons, in the following it will be assumed that the hadrons be pions (actually more than 80% are pions), so that the algebra considerably simplifies. Further simplification can be obtained by neglecting the sea contribution (i.e. $\Delta_T \bar{q} = \Delta_T s = 0$ and $\bar{q} = s = 0$) and considering only the range $0.1 < x < 0.3$. This is justified by the fact that the PDFs are expected to be considerably different from zero in the valence region, and the HERMES data show non-zero values in the range $0.05 < x < 0.3$. Assuming

$$D_u^{\pi^+} = D_d^{\pi^-} = D_1 \,, \ D_d^{\pi^+} = D_u^{\pi^-} = D_2 \,, \tag{35}$$

$$\Delta_T^0 D_u^{\pi^+} = \Delta_T^0 D_d^{\pi^-} = \Delta_T^0 D_1 \,, \ \Delta_T^0 D_d^{\pi^+} = \Delta_T^0 D_u^{\pi^-} = \Delta_T^0 D_2 \,, \tag{36}$$

and using Eq. (7), one gets for $\pi^+$ on a proton target:

$$A_{Coll}^{p,\pi^+} \simeq \frac{4\Delta_T u_v \Delta_T^0 D_1 + \Delta_T d_v \Delta_T^0 D_2}{4u_v D_1 + d_v D_2} \tag{37}$$

and for $\pi^-$:

$$A_{Coll}^{p,\pi^-} \simeq \frac{4\Delta_T u_v \Delta_T^0 D_2 + \Delta_T d_v \Delta_T^0 D_1}{4u_v D_2 + d_v D_1} \,. \tag{38}$$
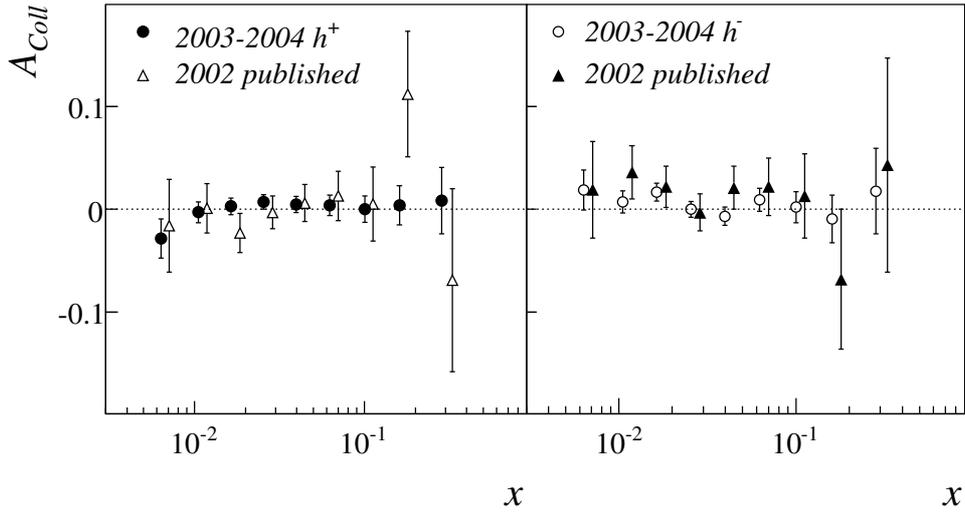
30

Figure 19: Collins asymmetry against $x$ for all positive (left) and all negative (right) hadrons from 2002 data [15] (triangles) and from 2003–2004 data (circles). The 2002 values are slightly shifted horizontally with respect to the measured value.

If, as suggested from the HERMES data, $\Delta_T^0 D_1 = -\Delta_T^0 D_2$, and taking $D_2 \simeq 0.5 D_1$, $d_v \simeq 0.5 u_v$, the previous expressions become

$$A_{Coll}^{p,\pi^+} \simeq \frac{\Delta_T u_v}{u_v} \frac{\Delta_T^0 D_1}{D_1} \tag{39}$$

and

$$A_{Coll}^{p,\pi^-} \simeq -\frac{4}{2.5} \frac{\Delta_T u_v}{u_v} \frac{\Delta_T^0 D_1}{D_1} \tag{40}$$
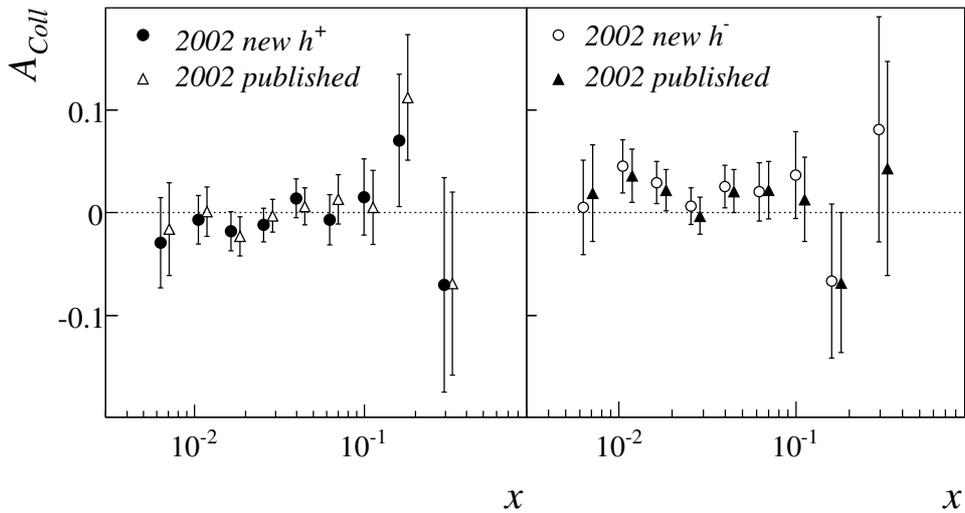


Figure 20: Collins asymmetry against $x$ for positive (left) and negative (right) hadrons from 2002 data. The triangles are the published results [15] and the circles the results of the new analysis. The published values are slightly shifted horizontally with respect to the measured value.
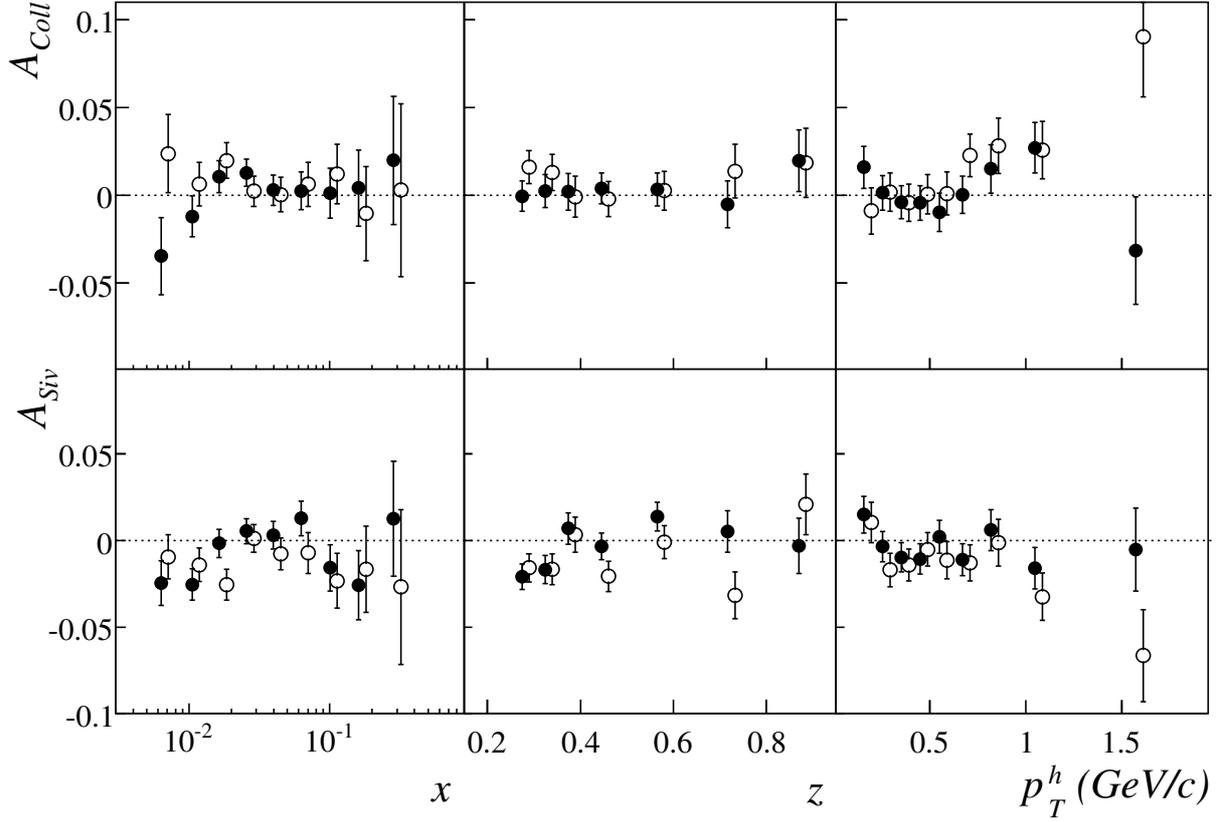
Figure 21: Overall results for Collins asymmetry (top) and Sivers asymmetry (bottom) against $x$, $z$ and $p_T^h$ for positive (full circles) and negative leading hadrons (open circles) from 2002, 2003, and 2004 data. Error bars are statistical only. In all the plots the open circles are slightly shifted horizontally with respect to the measured value.

respectively. As already stressed, the u-quark contribution is dominant.

For a deuteron target equations (37), (38), (39), and (40) become respectively

$$A_{Coll}^{d,\pi^+} \simeq \frac{\Delta_T u_v + \Delta_T d_v}{u_v + d_v} \frac{4\Delta_T^0 D_1 + \Delta_T^0 D_2}{4D_1 + D_2} \tag{41}$$

$$A_{Coll}^{d,\pi^-} \simeq \frac{\Delta_T u_v + \Delta_T d_v}{u_v + d_v} \frac{\Delta_T^0 D_1 + 4\Delta_T^0 D_2}{D_1 + 4D_2} \tag{42}$$

and

$$A_{Coll}^{d,\pi^+} \simeq \frac{3}{7} \frac{\Delta_T u_v + \Delta_T d_v}{u_v} \frac{\Delta_T^0 D_1}{D_1} \tag{43}$$

$$A_{Coll}^{d,\pi^-} \simeq -\frac{3}{4.5} \frac{\Delta_T u_v + \Delta_T d_v}{u_v} \frac{\Delta_T^0 D_1}{D_1} \tag{44}$$

Both the $\pi^+$ and the $\pi^-$ Collins asymmetries on the deuteron are proportional to $\Delta_T u_v(x) + \Delta_T d_v(x)$, therefore cancellation is expected to reduce considerably the effect which has been measured on the proton. As a matter of fact, assuming $\Delta_T d_v = 0$ (no limit on the size of $\Delta_T d_v$ is provided by the HERMES data) one derives relations between the Collins asymmetry measured by HERMES and COMPASS which are only marginally satisfied. Thus, the present precise data on $A_{Coll}^{d,\pi}$ should allow to extract $\Delta_T d_v$.
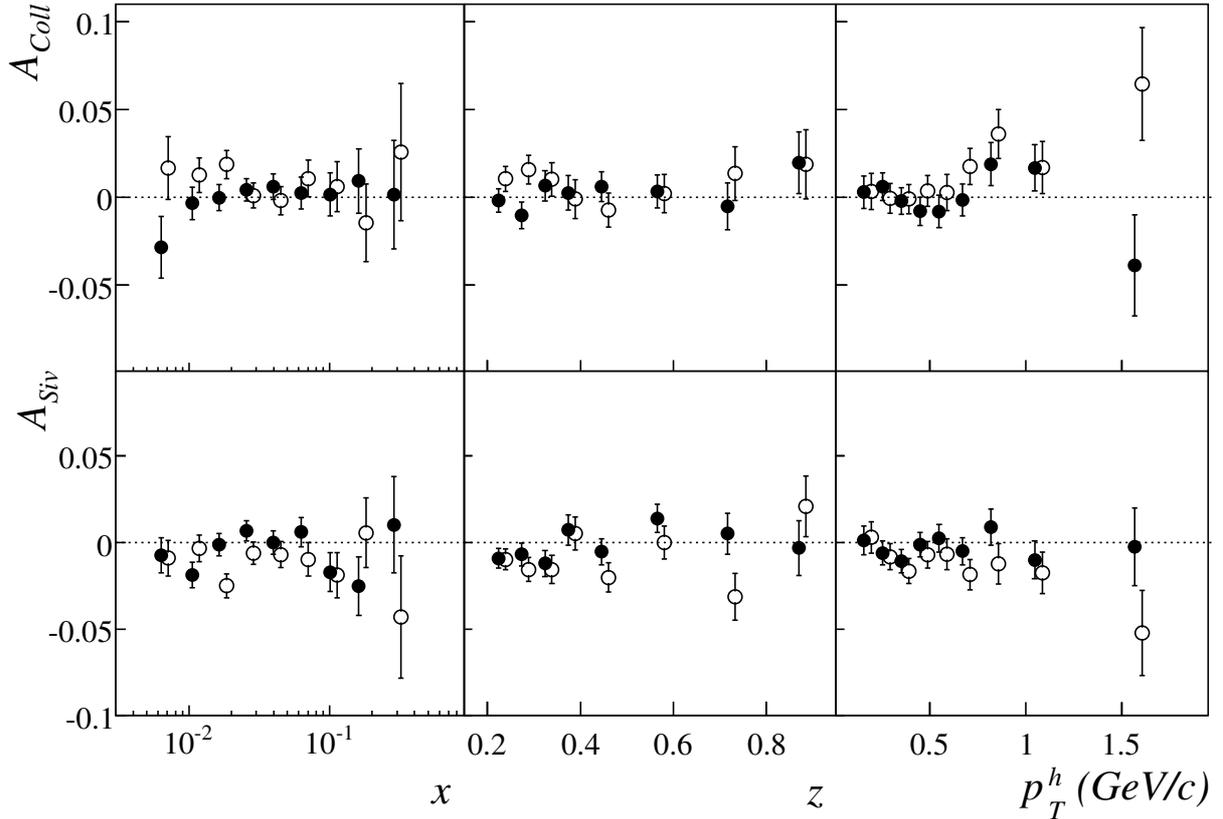
32

Figure 22: Overall results for Collins asymmetry (top) and Sivers asymmetry (bottom) against $x$, $z$ and $p_T^h$ for all positive (full circles) and all negative hadrons (open circles) from 2002, 2003, and 2004 data. Error bars are statistical only. In all the plots the open circles are slightly shifted horizontally with respect to the measured value.

This was not the case in so far. Three global analyses have been performed with the published data, trying to derive bounds on the transversity distributions and the Collins fragmentation functions. In Ref. [46] the Soffer bound $|\Delta_T q| = (q + \Delta q)/2$ was used, a fit of the HERMES data set was performed, and the Collins functions were extracted. Two different scenarios for favoured and unfavoured Collins fragmentation functions were considered, but the fits always favoured a relation $\Delta_T^0 D_1 \sim -\Delta_T^0 D_2$. The comparison of the fit results with the COMPASS data shows a fair agreement, as apparent from Fig. 23, although the data do not exhibit the trend with $x$ which is suggested by the model. The upper and lower curves in the figures correspond to the 1-$\sigma$ errors of the fitted parameters.

In Ref. [27] a chiral quark-soliton model was used for the transversity distributions, and the Collins fragmentation function was derived from a fit to the HERMES data, which do not constrain the $\Delta_T d$ distribution. A comparison with the present COMPASS results shows again a fair agreement (Fig. 24). The upper and lower curves in the figures correspond to the uncertainty in the Collins fragmentation functions as obtained from the fit. Independent extraction of the Collins function was performed by fitting the BELLE data. The result was found to be compatible with the one obtained fitting the HERMES data.

Similar results were obtained in Ref. [47]. Two different scenarios were used for transversity, either $\Delta_T q = \Delta q$, or the Soffer bound, and the Collins fragmentation functions were extracted from a fit to the HERMES data. The fits were very good in both cases. The extracted
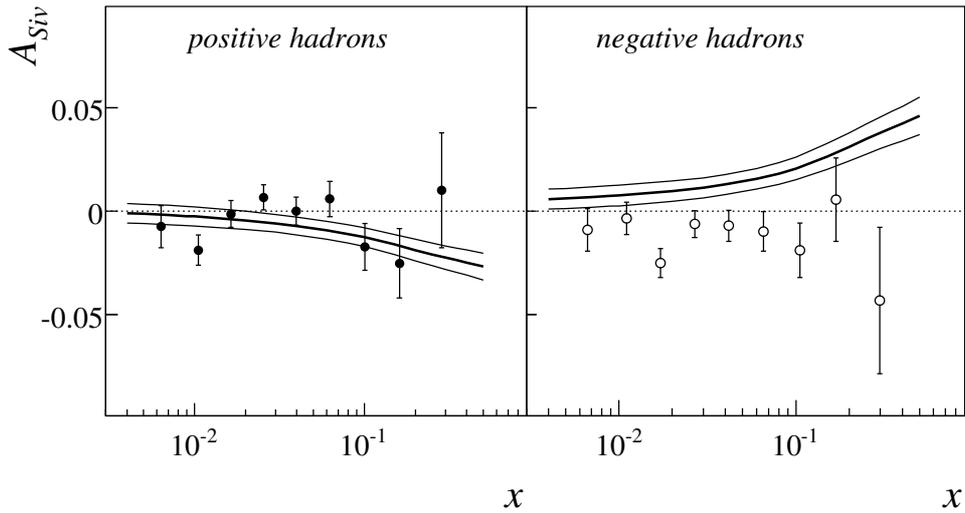
Figure 23: Comparison between the present results for positive (left) and negative (right) hadrons with the calculations of Ref. [46] (scenario 1).

Collins functions were then used to reproduce the published 2002 COMPASS data. The agreement is acceptable for both scenarios, as apparent from Fig. 25, although also in this case the expected increase of $A_{Coll}$ with increasing $x$ is not manifested by the COMPASS data. The upper and lower curves in all the figures correspond to 1-$\sigma$ deviations of the parameters. Also in this case the BELLE data are reproduced, and one can conclude that the Collins mechanism in SIDIS and in $e^+e^- \rightarrow$ hadrons are the same.

To summarise, the new data are compatible with the uncertainty bands given by the phenomenological calculations, but the trend of the data with $x$ is not the one suggested by the central value of the calculations: this is a clear indication that the COMPASS data will surely help in constraining the parameters of the models.
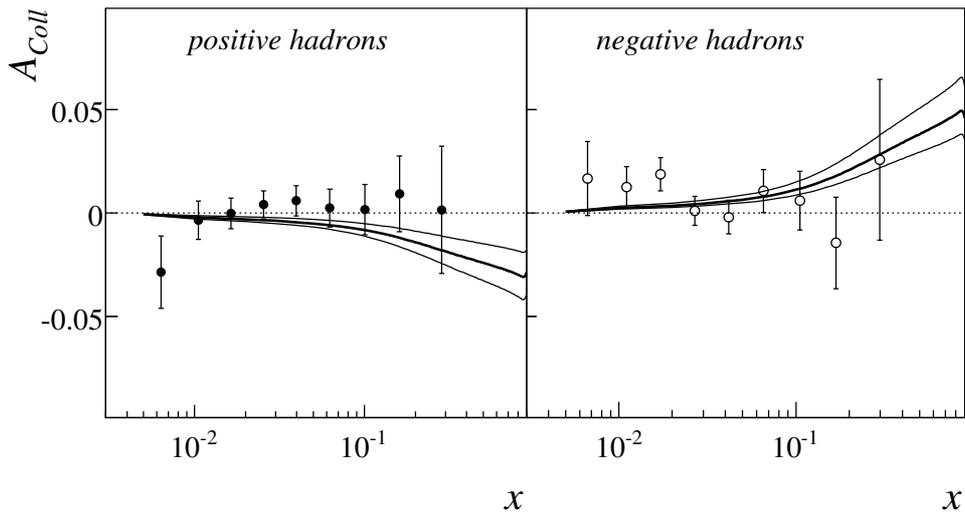


Figure 24: Comparison between the present results for positive (left) and negative (right) hadrons with the calculations of Ref. [27].
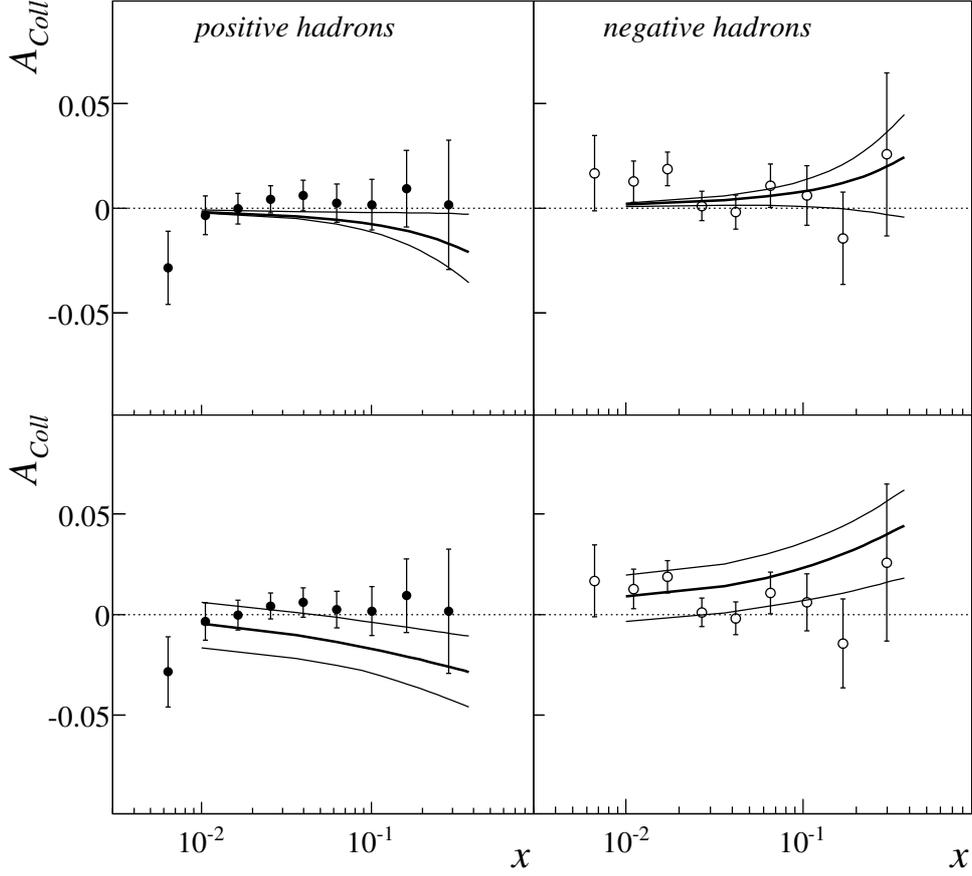
34

Figure 25: Comparison between the present results for positive (left) and negative (right) hadrons with the calculations of Ref. [47], where two scenarios were tested for transversity: $\Delta_T q = \Delta q$ was assumed in one scenario (upper figures), while $\Delta_T q = (q + \Delta q)/2$ was assumed for the calculations of the lower figures.

### 6.2.2 Sivers asymmetry

Also in this case it is useful to consider the expressions one obtains for $A_{Siv}$ in the hypothesis that all hadrons are pions. Again, the simplified analysis is restricted to the valence region.

Neglecting the sea contribution (i.e. $\Delta_0^T \bar{q} = \Delta_0^T s = 0$ and $\bar{q} = s = 0$ at all $x$) and assuming $D_u^{\pi^+} = D_d^{\pi^-} = D_1$ and $D_d^{\pi^+} = D_u^{\pi^-} = D_2$, on a proton target, from Eq. (14) one gets for $\pi^+$:

$$A_{Siv}^{p,\pi^+} \simeq \frac{4\Delta_0^T u_v D_1 + \Delta_0^T d_v D_2}{4 u_v D_1 + d_v D_2} \tag{45}$$

and for $\pi^-$:

$$A_{Siv}^{p,\pi^-} \simeq \frac{4\Delta_0^T u_v D_2 + \Delta_0^T d_v D_1}{4 u_v D_2 + d_v D_1} . \tag{46}$$

Assuming $D_2 \simeq 0.5 D_1$, $d_v \simeq 0.5 u_v$, the previous expressions become

$$A_{Siv}^{p,\pi^+} \simeq \frac{\Delta_0^T u_v}{u_v} \tag{47}$$

35

and

$$A_{Siv}^{p,\pi^-} \simeq \frac{2\Delta_0^T u_v + \Delta_0^T d_v}{2.5 u_v} \tag{48}$$

respectively. Since the Sivers asymmetries for $\pi^-$ as measured by HERMES is about zero, in this very simplified treatment it follows that

$$\Delta_0^T d_v = -2\Delta_0^T u_v . \tag{49}$$

For a deuteron target the Sivers asymmetries can be written as

$$A_{Siv}^{d,\pi^+} \simeq \frac{\Delta_0^T u_v + \Delta_0^T d_v}{u_v + d_v} \tag{50}$$

and

$$A_{Siv}^{d,\pi^-} \simeq \frac{\Delta_0^T u_v + \Delta_0^T d_v}{u_v + d_v} \tag{51}$$

which implies $A_{Siv}^{d,\pi^+} \simeq A_{Siv}^{d,\pi^-}$. The approximatively zero Sivers asymmetries for positive and negative hadrons observed in COMPASS require

$$\Delta_0^T d_v \simeq -\Delta_0^T u_v , \tag{52}$$

a relation which is also obtained in some models.

From Eq.(47), (48), and (49), a relation between the Sivers asymmetry measured by COMPASS and those measured by HERMES can be derived

$$A_{Siv}^{d,\pi^+} \simeq A_{Siv}^{d,\pi^-} \simeq -\frac{A_{Siv}^{p,\pi^+}}{1.5} \tag{53}$$

which is only marginally satisfied by the data.

Also the Sivers data have been looked upon independently by three different groups. In Ref. [26] a fit of the HERMES data was performed, on the assumption that $\Delta_0^T d(x) = -\Delta_0^T u(x)$. A good agreement with the HERMES data was obtained, and a zero asymmetry in case of a deuterium target was predicted, as shown in Fig. 26. The curves in the figure indicate the expected size of the effect on $A_{Siv}$ of the $1/N_c$-corrections. The COMPASS data fall well within the band resulting from the model.

The authors of Ref. [48] could estimate the Sivers functions by fitting both the HERMES and the published COMPASS data getting $\Delta_0^T d_v \simeq -\Delta_0^T u_v$. Leading Order MRST01 sets of unpolarised distribution functions [49] were used, together with Kretzer's set of fragmentation functions [50]. A very good agreement with the experimental data was reached, as apparent from Fig. 27, where the upper and lower curves correspond to 1-$\sigma$ deviation of the parameters. In this model the $z$ and $p_T^h$ dependence of the single spin asymmetries are also well described.

In Ref. [46] it was assumed that the final hadron transverse momentum is the transverse momentum in the Sivers function, i.e. a collinear fragmentation was assumed. GRV98 leading order distribution functions [51] were used, along with Kretzer's fragmentation functions. The fit of the HERMES data is very good, and gave as a result $\Delta_0^T d_v \simeq -\Delta_0^T u_v$, but the prediction for COMPASS are not in agreement with the new data, as shown in Fig. 28. The upper and lower curves in the figures correspond to 1-$\sigma$ errors in the fitted parameters. Here again, a new global fit using the deuteron data should be able to extract the Sivers function for the d-quark and improve the agreement with the data.

Very recently, the smallness of the Sivers asymmetry for positive and negative hadrons on the deuteron has been interpreted as evidence for the absence of gluon orbital angular momentum in the nucleon [52].
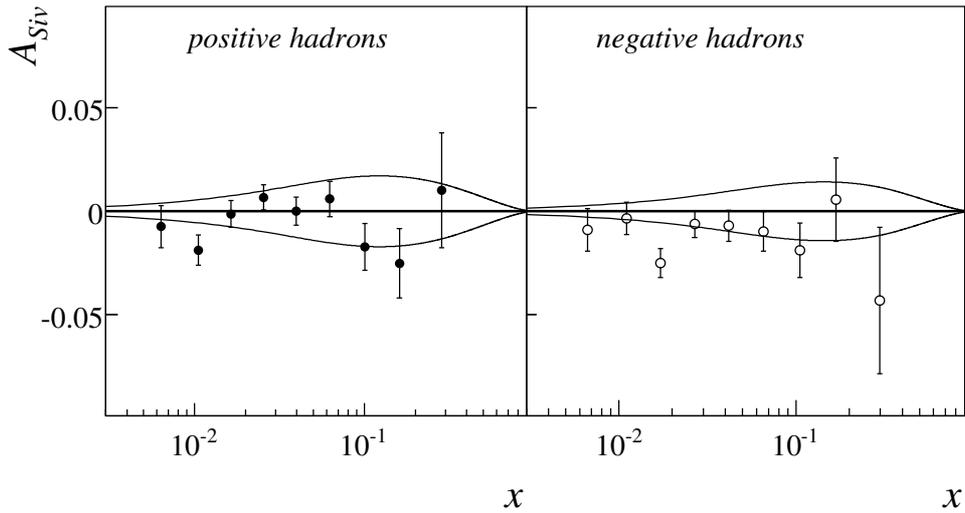
36

Figure 26: Comparison between the present results for positive (left) and negative (right) hadrons with the calculations of Ref. [26].

## 7   Conclusions

After providing the very first SIDIS data on transverse spin asymmetries on a transversely polarised deuteron target, COMPASS now publishes the overall results from the data collected in 2002, 2003, and 2004, increasing the statistics as compared to the published 2002 data by a factor of $\sim 7$, so that even at large $x$ the errors on the measured asymmetries are only a few percent.

All the measured asymmetries are small, mostly compatible with zero within the measurement errors. Presently, the most likely interpretation, taking into account the corresponding measurements of the HERMES collaboration on a proton target, is that in the COMPASS isoscalar target there is a cancellation between the proton and the neutron asymmetries. Also,
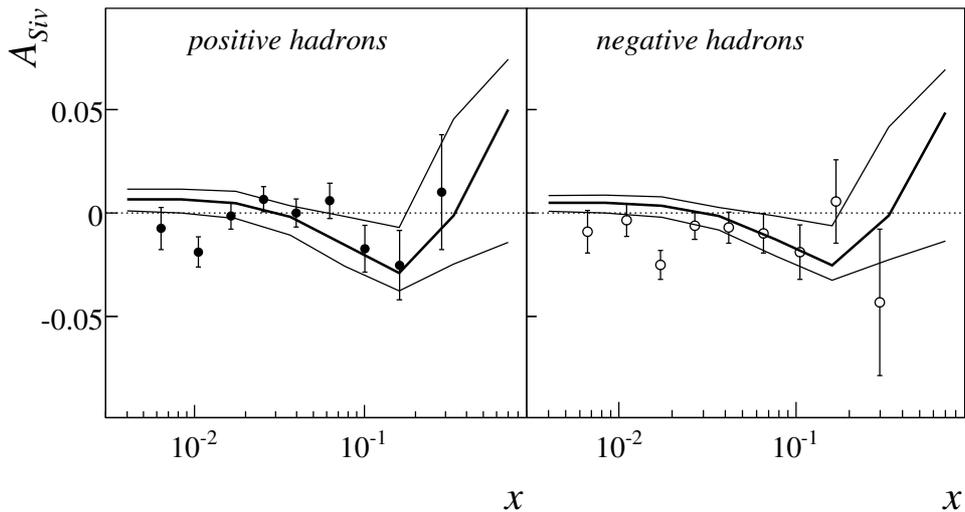


Figure 27: Comparison between the present results for positive (left) and negative (right) hadrons with the calculations of Ref. [48].
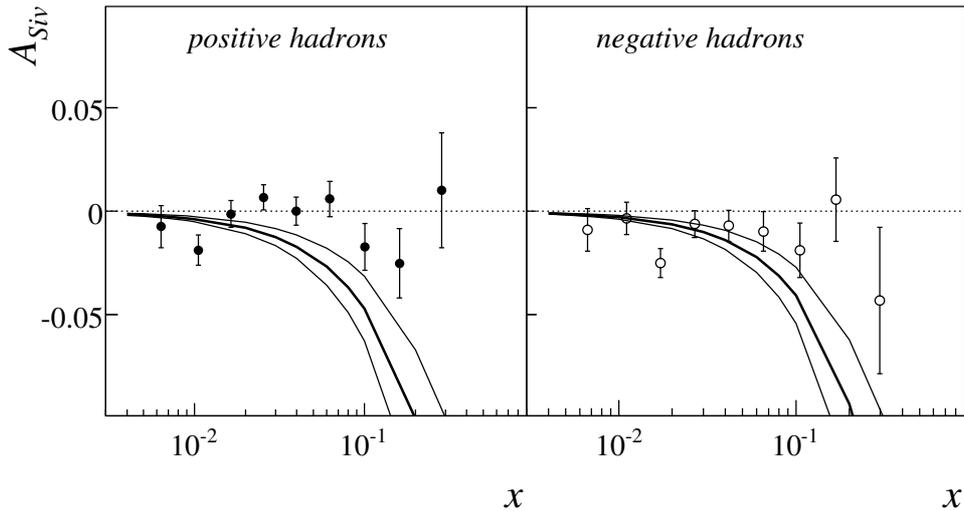
Figure 28: Comparison between the present results for positive (left) and negative (right) hadrons with the calculations of Ref. [46].

the independent evidence provided by the BELLE data that the Collins effect is a real physical mechanism guarantees that the transversity distributions $\Delta_T q(x)$ can be extracted from the single spin asymmetries measured in SIDIS. A global analysis of all the presently available data is now mandatory, and the inclusion of the new precise deuteron data from COMPASS will surely allow to provide first estimates of the down quark transversity distribution $\Delta_T d$ and of the Collins fragmentation functions $\Delta_T^0 D$. Already now the COMPASS data for the Sivers asymmetry provide convincing evidence on the cancellation of the u and d quark Sivers distribution functions.

It has to be stressed, however, that the measured effects are rather small, of the order of a few per cent at most, and that flavour separation requires much larger statistics than presently available. Also, within the present errors, the physics interpretation is not straightforward and has led to some surprises. The present data are of fundamental importance because they have opened up the road to transverse momentum dependent distribution and fragmentation functions, but they will by no means suffice to determine these new functions. New data are needed, and particularly, new proton data. HERMES is still finalising the analysis of their 2005 proton run, which will double the statistics of their analysed data. The BELLE Collaboration is producing more and more accurate data on the Collins fragmentation function. In the near future, COMPASS plans proton runs, which should result in particularly reduced error bars at large $x$, thanks to the much improved geometrical acceptance of the spectrometer which is obtained using the new COMPASS polarised target magnet. A global analysis will then again be necessary, and from all those measurements it should be able to provide the u and d quark transversity distributions.

## 8  Acknowledgement

38

## References

[1] G. Bunce *et al.*, Phys. Rev. Lett. **36** (1976) 1113.

[2] G.L. Kane *et al.*, Phys. Rev. Lett. **41** (1978) 1689.

[3] see, f.i., A. Efremov and O. Teryaev, Sov. J. Nucl. Phys. **39** (1984) 962, and the papers of the Lund team on $\Lambda$ polarisation.

[4] J. Antille *et al.*, Phys. Lett. B **94** (1980) 523.

[5] V.D. Apokin *et al.*, in 'Proceedings of the 7-th International Symposium on High Energy Spin Physics, Protvino, USSR, 1986 (Institute of High Energy Physics, Serpukhov, USSR, 1987) Vol 2, pag. 83.

[6] The Fermilab E704 Collaboration, A. Bravar *et al.*, Phys. Rev. Lett. **77** (1996) 2626.

[7] European Muon Collaboration, J. Ashman *et al.*, Phys. Lett. B **206** (1988) 364; Nucl. Phys. B **328** (1989) 1.

[8] J.P. Ralston and D.E. Soper, Nucl. Phys. B **152** (1979) 109.

[9] X. Artru and M. Mekhfi, Z. Phys. C **45** (1990) 669.

[10] R.L. Jaffe and X. Ji, Phys. Rev. Lett. **67** (1991) 552.

[11] J. Collins, Nucl. Phys. B **396** (1993) 161.

[12] G. Bunce *et al.*, Part. World **3** (1993) 1.

[13] The HELP Collaboration, B. Vuaridel *et al.*, CERN reports LEPC 93-14, LEPC/P7 (1993).

[14] The HERMES Collaboration, A. Airapetian *et al.*, Phys. Rev. Lett. **94** (2005) 012002.

[15] The COMPASS Collaboration, V. Y. Alexakhin *et al.*, Phys. Rev. Lett. **94** (2005) 202002.

[16] V. Barone and P.G. Ratcliffe, Phys. Rept. **359** (2002) 1.

[17] R.L. Jaffe and X. Ji, Nucl. Phys. B **375** (1992) 527.

[18] A. Kotzinian, Nucl. Phys. B **441** (1995) 234.

[19] P.J. Mulders and R.D. Tangerman, Nucl. Phys. B **461** (1996) 197.

[20] X. Artru, "The Transverse Spin", Proceedings of 10th Rhodanien Seminar, hep-ph/0207309.

[21] D. Sivers, Phys. Rev. D **41** (1990) 83

[22] S. J. Brodsky, D. S. Hwang and I. Schmidt, Phys. Lett. B **553** (2003) 223.

[23] J. C. Collins, Phys. Lett. B **536** (2002) 43.

[24] A. V. Belitsky, X. Ji and F. Yuan, Nucl. Phys. B **656** (2003) 165.

[25] D. Boer and P.J. Mulders, Phys. Rev. D **57** (1998) 5780.

[26] J. C. Collins *et al.*, Phys. Rev. D **73** (2006) 014021.

[27] A. Efremov *et al.*, Phys. Rev. **D73** (2006) 094025.

[28] The COMPASS Collaboration, E. S. Ageev *et al.*, Phys. Lett. B **633** (2006) 25.

[29] The COMPASS Collaboration, E. S. Ageev *et al.*, Phys. Lett. B **612** (2005) 154; the COMPASS Collaboration, V. Y. Alexakhin *et al.*, "The Deuteron Spin Dependent Structure Function $g_1^d$ and its First Moment", in preparation.

[30] The COMPASS Collaboration, "The COMPASS experiment at CERN", in preparation.

[31] J. Ball *et al.*, Nucl. Inst. Meth. A **498** (2003) 101.

[32] The Spin Muon Collaboration, D. Adams *et al.*, Nucl. Instrum. Meth. A **437** (1999) 23.

[33] Y. Giomataris *et al.*, Nucl. Inst. Meth. A **376** (1996) 29; F. Kunne, Nucl. Phys. A **721** (2003) 1087c.

[34] F. Sauli, Nucl. Inst. Meth. A **386** (1997) 531; B. Ketzer *et al.*, IEEE Trans. Nucl. Sci. **49** (2002) 2403.

[35] V.N. Bychkov *et al.*, Nucl. Inst. and Meth. A **556** (2006) 66.

[36] E. Albrecht *et al.*, Nucl. Inst. Meth. A **504** (354) 2003.

[37] C. Bernet *et al.*, Nucl. Inst. Meth. A **550** (2005) 217.

[38] L. Schmitt *et al.*, IEEE Trans. Nucl. Sci. **51** (439) 2004.

[39] for all the COMPASS off-line pakages see
http://wwwcompass.cern.ch/compass/software/offline/welcome.html#software.

[40] R. Brun and F. Rademakers, Nucl. Instrum. Meth. A **389** (1997) 81. See also
http://root.cern.ch/.

[41] HEPDATA: The Durham HEP Database,
http://durpdg.dur.ac.uk/HEPDATA/index.html.

[42] A.V. Efremov, Annalen Phys. **13** (2004) 651.

[43] F. James, MINUIT, CERN Program Library Long Writeup D506,
http://wwwasdoc.web.cern.ch/wwwasdoc/WWW/minuit/minmain/minmain.html.

[44] The Belle Collaboration, K. Abe *et al.*, Phys. Rev. Lett. **96** (2006) 232002.

[45] A. Ogawa *et al.*, "Spin dependent fragmentation function at Belle," arXiv:hep-ex/0607014.

[46] W. Vogelsang and F.Yuan, Phys. Rev. **D72** (2005) 054028.

[47] M. Anselmino *et al.*, RICH + AGS annual Users' Meeting June 6, 2006,
www.bnl.gov/rhic_ags/users_meetings/workshops/basp, and paper in preparation.

[48] M. Anselmino *et al.*, Phys. Rev. D **72** (2005) 094007.

[49] A. D. Martin *et al.*, Phys. Lett. B **531** (2002) 216.

[50] S. Kretzer, "Fragmentation functions from flavour-inclusive and flavour-tagged e+ e-
Phys. Rev. D **62** (2000) 054001.

[51] M. Glück, E. Reya and A. Vogt, Z. Phys. C **67** (1995) 433.

[52] S. J. Brodsky and S. Gardner, "Evidence for the Absence of Gluon Orbital Angular Momentum in the Nucleon", arXiv:hep-ph/0608219.